









Rare t(X;14)(q28;q32) translocation reveals link between *MTCP1* and chronic lymphocytic leukemia

Janek S. Walker ^{1,10}, Zachary A. Hing^{1,10}, Steven Sher¹, James Cronin^{1,2}, Katie Williams¹, Bonnie Harrington¹, Jordan N. Skinner¹, Casey B. Cempre¹, Charles T. Gregory¹, Alexander Pan¹, Max Yano¹, Larry P. Beaver¹, Brandi R. Walker¹, Jadwiga M. Labanowska³, Nyla A. Heerema³, Krzysztof Mrózek⁴, Jennifer A. Woyach ¹, Amy S. Ruppert ¹, Amy Lehman⁵, Hatice Gulcin Ozer⁶, Vincenzo Coppola ^{7,8}, Pearlly Yan ¹, John C. Byrd ^{1,9}, James S. Blachly ^{1,6} & Rosa Lapalombella ¹✉

Rare, recurrent balanced translocations occur in a variety of cancers but are often not functionally interrogated. Balanced translocations with the immunoglobulin heavy chain locus (*IGH*; 14q32) in chronic lymphocytic leukemia (CLL) are infrequent but have led to the discovery of pathogenic genes including *CCND1*, *BCL2*, and *BCL3*. Following identification of a t(X;14)(q28;q32) translocation that placed the mature T cell proliferation 1 gene (*MTCP1*) adjacent to the immunoglobulin locus in a CLL patient, we hypothesized that this gene may have previously unrecognized importance. Indeed, here we report overexpression of human *MTCP1* restricted to the B cell compartment in mice produces a clonal CD5⁺/CD19⁺ leukemia recapitulating the major characteristics of human CLL and demonstrates favorable response to therapeutic intervention with ibrutinib. We reinforce the importance of genetic interrogation of rare, recurrent balanced translocations to identify cancer driving genes via the story of *MTCP1* as a contributor to CLL pathogenesis.

¹Division of Hematology, Department of Internal Medicine, The Ohio State University, Columbus, OH, USA. ²Department of Veterinary Biosciences, The Ohio State University, Columbus, OH, USA. ³Department of Pathology, The Ohio State University, Columbus, OH, USA. ⁴The Ohio State University Comprehensive Cancer Center, Clara D. Bloomfield Center for Leukemia Outcomes Research, The Ohio State University, Columbus, OH, USA. ⁵Center for Biostatistics, The Ohio State University, Columbus, OH, USA. ⁶Department of Biomedical Informatics, The Ohio State University College of Medicine, Columbus, OH, USA. ⁷Department of Cancer Biology and Genetics, The Ohio State University College of Medicine, Columbus, OH, USA. ⁸Genetically Engineered Mouse Modeling Core, The Ohio State University and Arthur G. James Comprehensive Cancer Center, Columbus, OH, USA. ⁹Division of Pharmaceutics and Pharmacology, College of Pharmacy, The Ohio State University, Columbus, OH, USA. ¹⁰These authors contributed equally: Janek S. Walker, Zachary A. Hing. ✉email: rosa.lapalombella@osumc.edu

Chronic lymphocytic leukemia (CLL) is the most prevalent adult leukemia in Western countries and is characterized by a mature B-cell phenotype¹. In contrast to other chronic adult leukemias, CLL is not primarily fusion/proto-oncogene driven. Instead, CLL pathogenesis likely begins with a lymphoid primed progenitor cell that becomes transformed at either a pre- or post-germinal center developmental stage bearing *IGHV* mutational status and a distinct epigenetic pattern corresponding to points along normal B-cell development^{2–5}.

During CLL transformation, loss or gain of genetic material then appears to be a key determinant of disease phenotype and clinical outcome, with chromosomal aberrations such as deletions in regions of chromosomes 11, 13, or 17 [del(11q23), (del(13q14), or del(17p13), respectively], or a gain in copy number of chromosome 12 (trisomy 12) observed in up to 80% of patients^{6,7}. Alternatively, balanced translocations, specifically those including the immunoglobulin heavy chain locus (*IGH*; 14q32) resulting in constitutive overexpression of various proto-oncogenes in the B-cell compartment, occur far less frequently⁸. Despite their infrequency, molecular profiling of these rare rearrangements have revealed broad importance of previously un-recognized coding or non-coding genes critical to the pathogenesis of CLL. Practical application of this strategy facilitated understanding the role of the anti-apoptotic protein *BCL2* in CLL. While abundantly present in follicular lymphoma and diffuse large B-cell lymphoma (DLBCL), the t(14;18)(q32;q21) translocation—involving the *IGH* locus and the *BCL2* gene—is a rare event in CLL (1–2% of cases)^{9,10}. Yet even in absence of a t(14;18)(q32;q21) rearrangement, it was found that *BCL2* mRNA was over-expressed in virtually all CLL patients compared to normal B-cells¹¹. Work to determine mechanisms driving this abnormality later revealed microRNAs *miR-15/16* as leading posttranscriptional regulators of *BCL2* and loss of *miR-15/16* as a result of 13q14 deletions substantially associate with elevated *BCL2* expression in CLL^{12–14}. The pathogenic importance of this discovery subsequently led to a greater understanding of CLL disease biology and mechanisms resulting in the dramatic clinical activity demonstrated by the BH3-mimetic venetoclax¹⁵; ultimately contributing to the overall improvement in the therapeutic management of CLL.

Along this principle, we have identified a CLL patient with a previously undescribed t(X;14)(q28;q32) translocation, which leads to co-localization of the mature T cell proliferation 1 (*MTCP1*) coding region with the *IGH* locus, a situation analogous to the translocation of *BCL2*. Despite no known role in CLL, we found elevated *MTCP1* mRNA expression in CLL cells compared to normal B cells and that increased *MTCP1* expression in CLL patients portends poor outcomes to chemoimmunotherapy. Further interrogating this phenomenon we demonstrate the capacity for *MTCP1* to initiate development of an aggressive murine CLL-like leukemia, revealing *MTCP1* as a target for exploring the pathogenic mechanisms driving CLL. This discovery produces an in vivo model to investigate these unexplored mechanisms and to evaluate therapeutic strategies with optimal translatability to the clinical setting.

Results

t(X;14)(q28;q32) translocation identified in CLL. The Xq28 locus containing *MTCP1* is bicistronic, encoding two distinct transcripts as a result of an ancient insertion event¹⁶. *MTCP1* (previously termed p13 *MTCP1*) lies within the first intron of an unrelated gene *CMC4* (previously termed p8 *MTCP1*), with the two genes' distinct open reading frames preceded by a shared 5' UTR (Supplementary Fig. 1A). Previous studies, using X-ray diffraction to estimate the crystal structure of both p13 *MTCP1* and p14 *TCL1A* proteins^{17–19}, describe a high degree of overlap

between both amino acid sequence and 3-dimensional protein conformation—highlighted by an eight-strand beta barrel tertiary structure remarkably unique to this family of proteins (Supplementary Fig. 1B)^{20–22}. Translocations involving the *MTCP1* (Xq28) and T-cell receptor (*TCRA/D*) genes have been shown to induce constitutive *MTCP1* overexpression and is a leukemic driving event in T-cell-prolymphocytic leukemia (T-PLL)^{23–26}. To date, *MTCP1* on the Xq28 locus has not been implicated in B-cell leukemia or lymphoma.

To explore a potential role for Xq28 translocations in B-cell malignancies, we screened metaphase karyotypes of 1744 cases suspected of CLL and identified eight (0.45%) with Xq28 rearrangements (Table 1). One case, a 59 year old female patient with *IGHV*-unmutated CLL, harbored a reciprocal t(X;14)(q28;q32) translocation, possibly involving the *MTCP1* coding region and the *IGH* locus. To confirm this we performed fluorescent in-situ hybridization (FISH) analysis with probes directed against the *IGH* (3' red; 5' green) and *MTCP1* (red) loci on metaphases. This showed that 5' *IGH* moved to the X chromosome (Fig. 1A) and *MTCP1* was indeed translocated to the 5' end of the *IGH* locus (Fig. 1B). Combining the two probes demonstrated the *MTCP1* and 3'*IGH* probes co-localized on a chromosome 14, consistent with the results with *MTCP1* by itself, and 5' (green) *IGH* was on an X chromosome (Fig. 1C).

We then evaluated *MTCP1* mRNA expression in CLL-B cells without any known Xq28 rearrangements and found ~2 fold higher *MTCP1* mRNA transcripts in these CLL cells compared to naïve- or memory-B cells (Fig. 1D). A similar trend with *CMC4* in CLL cells was also observed (Supplementary Fig. 1C). To interrogate the clinical significance of *MTCP1* mRNA expression in CLL, we conducted a retrospective analysis on *MTCP1* expression in CLL patients from two independent chemoimmunotherapy trial study cohorts for which microarray data have been previously reported (CALGB '9712' and '10101')^{27,28}. Here, we correlated CLL risk factors with *MTCP1* expression using baseline characteristics obtained at time of treatment initiation (Table 2). When stratified into quartiles by *MTCP1* expression we observed a similar distribution between sexes and high-risk CLL cofactors including age, performance status, cytogenetic evaluation, *IgHV* mutation status, and Zap-70 methylation; with the exception of elevated blood lymphocyte counts (WBC) and advanced Rai stage at diagnosis skewing towards patients with higher *MTCP1* expression (Q2-4). As a single continuous variable, a 2-fold increase in *MTCP1* expression was also found to associate with shorter progression-free survival (PFS) when adjusting for study cohort ($p = 0.03$; Supplementary Table 1). To illustrate this association, we plotted PFS by *MTCP1* expression quartile for all patients and for each study cohort; visualizing that patients with the lowest expression (Q1) tended to have longer PFS (Fig. 1E; Supplementary Fig. 1D, E). Further, as *IgHV* mutation status is a strong predictor of outcome in CLL¹, a bivariate analysis including continuous *MTCP1* expression and *IgHV* status found a 2-fold increase in *MTCP1* expression was prognostic for PFS independent of *IgHV* status ($p = 0.03$; Supplementary Table 2).

B cell-specific *MTCP1* overexpression drives a spontaneous and lethal leukemia. Due to the proposed conservation of structure and function between p13 *MTCP1* and p14 *TCL1A*, the fungible role of both in T-PLL pathogenesis, the known role of *TCL1A* in CLL²⁹, identification of Xq28 translocations in CLL with unresolved significance, and the apparent influence of *MTCP1* expression on CLL outcomes, we hypothesized *MTCP1* acts as a leukemogenic co-stimulator—revealing an unrecognized factor in CLL pathogenesis. To test this hypothesis, we generated

Table 1 Clinical demographics for suspected CLL cases with Xq28 rearrangements.

Age (years)	Sex	Diagnosis	IGHV	Treated	Complexity	Karyotype ^a
59 ^A	F	CLL	Unmutated	No	2	47,XX,+12[17]/47,idem,t(X;14)(q28;q32)[2]/46,XX[2].ish t(X;14)(5' IGH+;3' IGH+)
59	F	CLL	ND	Yes	3	46,X,t(X;12)(q28;q13),t(3;19)(q28;q13.1),add(20)(q11.2)[9]/46,XX[10]/nonclonal[2].ish t(3;19)(BCL6+, BCL3+;BCL6-,BCL3-)
71	M	CLL	Unmutated	yes	>6	46,XY,del(6)(q13)[cp2]/45,sl,der(6)ins(6;?)p(21;?)del(6)(q21),der(8)t(8;15)(p21;q15),-15,idic(16)(p11.2),add(17)(p11.2)[cp19]/45,t(X;12)(q28;q13),-Y,+8,add(9)(q22),del(11)(q21),-22[cp2]/46,XY[2]/nonclonal[1].ish add(17)(TP53-)
74	F	CLL	Mutated	Yes	4	46,XX,del(6)(q15q21)[9]/46,idem,t(X;8)(q28;q22),inv(11)(p15q23)[cp3,one is 4n]/nonclonal w/clonal abnormalities[1]/46,XX[16]
59	M	Diffuse Large B-Cell Lymphoma	ND	No	>6	47,XY,der(X)t(X;8)(q28;q24.2)ins(X;?)q28;?,dup(1)(q21q42),dup(2)(q31q35),t(3;9)(q27;q32),del(7)(q22q32),der(8)t(X;8)(q28;q24.2),+12,der(12)t(12;13)(q24.3;q22)x2,der(13)t(12;13)(q24.3;q12),t(14;19)(q32.3;q13.2)[cp16]/53,sl,+der(X)t(X;8)ins(X;?),+4,+5,-del(7),+11,+der(12)t(12;13)[cp3]/46,XX[1]
60	M	CLL	Unmutated	Yes	>6	44,XY,del(9)(p22),psu dic(17;6)(p13;q21),dic(18;20)(p11.2;p11.2)[11]/45,sl,add(X)(q28),+add(9)(p22),-del(9)(p22),dic(15;21)(p11.2;p11.2),+18,-dic(18;20),+20,+mar1[2]/90-91,sdl1x2,+add(X),+add(X),-Y,add(9)(q22)x4,-add(9)(p22),-add(9)(p22),+mar2[2]/44,sl,del(13)(q12q21.2)[5]/nonclonal w/clonal abnormalities[1]
64	F	CLL	Unmutated	yes	>6	60-79<4n>,XX,-X,-X,add(1)(q21)x2,add(3)(q29)x2,-4,-4,-6,-6,-8,-8,-9,-9,-13,-13,-14,psu dic(17;5)(p11.2;p13)x2,-18,add(18)(q23)x2,+mar1,+mar2x2[cp4]/72-80,sl,add(20)(q13.3),-mar1,+mar4[cp7]/58-78,sdl1,add(X)(q28)[cp2]/84-94,sdl1,+2,+7,+16,+19[cp2]/nonclonal w/ clonal abnormalities[5]
56	M	CLL	Unmutated	no	4	45,Y,der(X)(Xpter->Xq28::11q12->11q13::1q32->1qter),der(1)t(1;11)(q32;q13),der(11)(?::11p15.5->11q12::Xq28->Xqter),-21[cp2]/46,XY[16]/nonclonal[4].ish der(X)(CCND1+),der(1)(ATM+)

^aXq28 rearrangement indicated in bold.

^AFISH analysis of CLL cells from this patient are depicted in Fig. 1.

a transgenic mouse model expressing recombinant human *MTCP1* under the control of a VH promoter-IgH-E μ enhancer, targeting transgene expression to immature and mature B cells (E μ -MTCP1; Supplementary Fig. 2A). Transgenic founders (Z36 and Z20) on the C57/BL6NTac background were bred to establish separate mouse lines, with successful passage of the *MTCP1* transgene to progeny confirmed via PCR (Supplementary Fig. 2B). To further confirm transgene integration into founder mice, we performed targeted locus amplification³⁰ in the established founder lines (Supplementary Fig. 2C, D). For both Z36 and Z20 founder lines, the genomic region between the 5' and 3' region of the integration site was deleted during the integration event. No structural variations were detected in the transgenic sequences, and >10 copies of the transgene integrated in each founder line.

CLL is characteristically defined as an accumulation of CD45⁺ B lymphocytes with phenotypic expression of cell-surface markers CD5, CD19, and CD23, with dim—or intermediate—expression of CD45R (B220)¹. To evaluate the potential of the E μ -MTCP1 model to develop a leukemia resembling a CLL-like phenotype, littermate mice from Z36 and Z20 founder lines were followed monthly via flow cytometry analysis of the blood. Gating on CD45⁺ cells and probing for CD19⁺/CD5⁺ and CD19⁺/B220^{dim} cell populations, a progressive expansion of circulating CLL-like B-cells were detected as early as 5 months of age in both E μ -MTCP1 founder lines (Fig. 2A). The percentage of transgenic mice spontaneously developing a CLL-like leukemia were 70% and 28% for founder lines Z36 and Z20, respectively (Fig. 2B). Using detection of >20% CLL-like cells in the blood as a threshold for leukemia onset, E μ -MTCP1 founder lines Z36 and Z20

reached “diseased” status at a median time of 7.7 and 16.7 months, respectively (Fig. 2C). Regardless of type and severity of hematologic abnormality, the majority of Z36 and Z20 E μ -MTCP1 mice died spontaneously or met early removal criteria (ERC) due to evidence of clinical deterioration at a median time of 10.8 and 14.5 months, respectively—a significant reduction from the median lifespan observed in wildtype littermates (Fig. 2D, E). Notably, the progressive accumulation of CLL-like B cells in E μ -MTCP1 mice followed a similar trend to that observed in E μ -TCL1 mice (Supplementary Fig. 3A)—a widely used CLL mouse model which reliably (reported 95–100% penetrance) develops a CLL-like phenotype driven by over-expression of recombinant human *TCL1A* also under control of a VH promoter-IgH-E μ enhancer^{31,32}. A cohort of E μ -TCL1 mice in our laboratory maintained a similar median time to CLL-like leukemia onset with E μ -MTCP1 founder line Z36 and a similar median survival with E μ -MTCP1 founder line Z20 (Supplementary Fig. 3B, C). Evaluating only mice that developed a CLL-like phenotype by censoring animals at the time at which a T cell or myeloid cell abnormality was observed, a competing risk assessment estimated the median survival for founder lines Z36 and Z20 to be 12.4 months and 17.6 months, respectively (Supplementary Fig. 3D). While the estimated median survival of E μ -MTCP1 founder Z20 extended beyond that observed in E μ -TCL1 mice (14.1 months), we observed a significant reduction in time from leukemia onset to death in both Z36 and Z20 E μ -MTCP1 founder lines (4.10 months and 2.94 months, respectively), when compared to the E μ -TCL1 model (7.41 months; Supplementary Fig. 3E). Taken together, this evidence suggests that while the rate of CLL-like leukemia onset in Z20 lineage mice

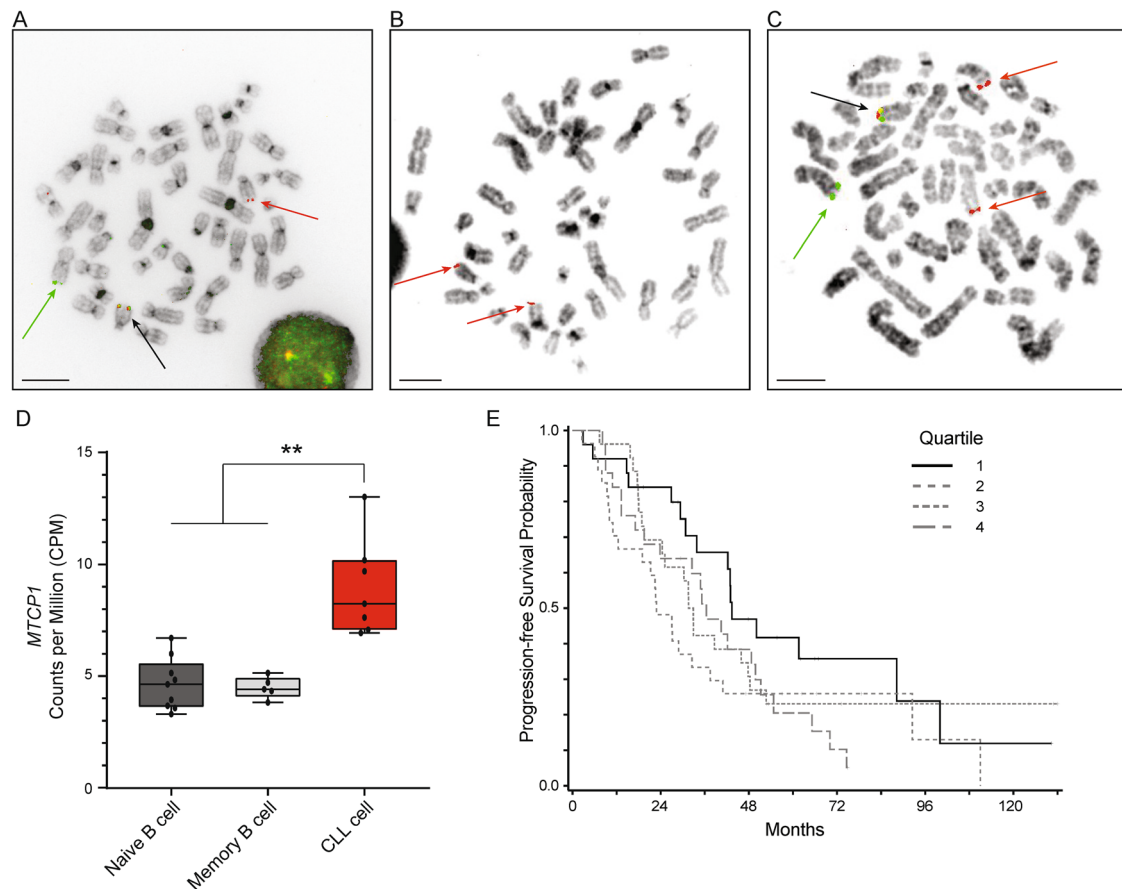


Fig. 1 MTCPI is expressed in CLL patients and is associated with poor outcomes. **A** Metaphase FISH was performed on CpG-stimulated CLL cells using the *IGH* break apart (3' red; 5' green) hybridization probes. Representative FISH analysis in one CLL patient harboring the t(X;14)(q28;q32) translocation showing the *IGH* probe has split with 5' (green) on an X chromosome and 3' (red) remaining on a chromosome 14. Images represent three independent tests. Scale bars are 10 μ m. **B** Metaphase FISH was performed on CpG-stimulated CLL cells using the *MTCPI* (red) hybridization probe. Representative FISH analysis in the patient from (**A**) showing the *MTCPI* loci are on an X chromosome and on distal 14q. Images represent three independent tests. **C** Metaphase FISH was performed on CpG-stimulated CLL cells combining the *IGH* (3' red; 5' green) and *MTCPI* (red) probes. Representative FISH analysis in the patient from (**A**) showing the *MTCPI* and 3' *IGH* probes co-localize on a chromosome 14 and 5' (green) *IGH* is on an X chromosome. Images represent three independent tests. **D** *MTCPI* mRNA expression is elevated in CLL cells (without any known Xq28 rearrangements) compared to naïve- or memory-B-cell subsets ($p = 0.0012$, $p = 0.0013$, respectively). Data obtained from the Blueprint database. Box elements reflect 2nd - 3rd quartile, center line reflects the median value, and whiskers reflect the distance from the upper and lower limit to the box elements. CLL cells - red/right, $n = 7$; naïve B cells - dark gray/left, $n = 9$; memory B cells - light gray/middle, $n = 5$. P value estimated using a two-tailed unpaired t test with Welch's correction. **E** Higher *MTCPI* expression in CLL patients identified with shorter progression-free survival (PFS) in chemoimmunotherapy trials. CLL patients from two independent study cohorts from Cancer and Leukemia Group B clinical trials (9712 and 10101; $N = 103$) were retrospectively analyzed. Patients were divided into quartiles: Q1 (solid line, $n = 25$), Q2 (medium-dash, $n = 27$), Q3 (short-dash, $n = 26$), and Q4 (long-dash, $n = 25$) according to *MTCPI* expression and PFS was visualized using the Kaplan-Meier method. As a continuous variable, the crude hazard ratio for a 2-fold increase in expression is 1.86 (95% CI: 0.97-3.55, $P = 0.06$) estimated from a Cox proportional hazards model. P value was determined via two-sided Wald test. No adjustments were made for multiple testing.

was significantly delayed in relation to Z36 lineage mice, upon CLL onset the kinetics of this CLL-like disease remained largely similar between the two founder lines.

A previously described hallmark of CLL B cells includes elevated expression of cytotoxic T-lymphocyte associated protein 4 (CTLA4)³³. Our group has demonstrated that unless co-stimulation is provided, CTLA4 is not normally found on the surface of human CLL cells and expression is restricted to the intracellular compartment³⁴. Using fluorescently labeled flow cytometry antibodies to detect both intracellular and surface CTLA4 in the blood from E μ -MTCPI mice, we found that, like human CLL and unlike E μ -TCL1 CLL-like cells, CTLA4 expression was restricted to the intracellular compartment (Supplementary Fig. 3F).

MTCPI driven leukemia recapitulates aggressive human CLL.

E μ -MTCPI mice meeting ERC due to CLL-like disease invariably presented with splenomegaly accompanied by abdominal lymphadenopathy (Fig. 3A). Histopathology evaluation revealed variable neoplastic infiltration of lymphoid tissues including robust splenic and lymphatic involvement with very modest presence in the marrow (Fig. 3B). Tumor cross sections exhibited variable degrees of F4/80 and B220-expressing infiltrates as detected by immunohistochemistry, with scant numbers of CD3⁺ mature, well-differentiated lymphocytes, which were interpreted as tumor-associated lymphocytes³⁵. Healthy mouse tissues were infiltrated and effaced by neoplastic populations resembling both small-to-intermediate-sized lymphocytes and larger histiocytoid round cells, similar to those previously reported for the E μ -TCL1 mouse model³¹.

Table 2 Association between *MTCP1* expression and baseline characteristics in CLL patients.

	All Patients N = 103	Quartile 1 Expression n = 25	Quartile 2 Expression n = 27	Quartile 3 Expression n = 26	Quartile 4 Expression n = 25	P value
Expression (Log 2)						NA
Median	9.02	8.52	8.91	9.11	9.33	
Range	8.16-10.26	8.16-8.70	8.78-9.02	9.03-9.19	9.20-10.26	
Study						0.28
9712	41 (40%)	7 (28%)	9 (33%)	12 (46%)	13 (52%)	
10101	62 (60%)	18 (72%)	18 (67%)	14 (54%)	12 (48%)	
Age						0.07
Median	62	62	55	61	66	
Range	34-83	42-81	34-77	38-83	46-79	
Hemoglobin						0.08
Median	12.8	11.9	13.2	13.2	11.7	
Range	5.5-16.9	5.5-15.1	9.9-16.9	8.2-15.5	6.6-15.1	
Missing/Unknown	6	0	1	1	4	
WBC (count ^{E-3} /μL)						0.03
Median	108.6	67.0	132.0	108.6	131.0	
Range	6.3-436.0	6.3-238.0	22.0-255.0	29.0-402.0	30.0-436.0	
Missing/Unknown	3	0	1	0	2	
Sex						0.66
Male	82 (80%)	20 (80%)	20 (74%)	20 (77%)	22 (88%)	
Female	21 (20%)	5 (20%)	7 (26%)	6 (23%)	3 (12%)	
Performance Status						0.29
0	61 (60%)	14 (56%)	12 (46%)	18 (69%)	17 (68%)	
1/2+	41 (40%)	11 (44%)	14 (54%)	8 (31%)	8 (32%)	
Missing/Unknown	1	0	1	0	0	
Rai Stage						0.47
I/II	63 (61%)	17 (68%)	18 (67%)	16 (62%)	12 (48%)	
III/IV	40 (39%)	8 (32%)	9 (33%)	10 (38%)	13 (52%)	
Cytogenetics Group						0.18
del(17p)/del(11q)	22 (24%)	7 (30%)	7 (30%)	2 (8%)	6 (26%)	
Other	71 (76%)	16 (70%)	16 (70%)	22 (92%)	17 (74%)	
Missing/Unknown	10	2	4	2	2	
IgHV Usage						0.77
Mutated	28 (31%)	7 (30%)	9 (38%)	5 (23%)	7 (33%)	
Unmutated	62 (69%)	16 (70%)	15 (63%)	17 (77%)	14 (67%)	
Missing/Unknown	13	2	3	4	4	
Zap-70 Methylation						0.95
<20%	80 (79%)	19 (76%)	21 (78%)	20 (80%)	20 (83%)	
≥20%	21 (21%)	6 (24%)	6 (22%)	5 (20%)	4 (17%)	
Missing/Unknown	2	0	0	1	1	

Next, we analyzed the immunophenotypic signature of B-cell subsets using established murine markers of B-cell development. Representative plots are depicted in Fig. 3C, including comparison to blood from wildtype littermates and Eμ-TCL1 mice. After gating out CD3⁺ T and CD11b⁺ myeloid populations, cells were visualized using CD19 and CD5 expression markers: a phenotypically homogeneous CD19⁺/CD5⁺ co-expression population (CLL-like cells) with marked expansion in the blood was observed in Eμ-MTCP1 mice but not wildtype littermates. Typically, lymphocytes of significantly diseased Eμ-MTCP1 mice were composed of >60% CD19⁺/B220^{dim} B cells. CLL-like cells and maturing B cells (CD19⁺/CD5⁻) were further dissected according to CD21 and IgM expression to identify CD21⁺/IgM⁺ marginal zone/marginal zone progenitor (MZ/MZP) B cells, CD21^{int}/IgM^{dim} follicular B cells, and CD21⁻/IgM⁻ or CD21⁻/IgM⁺ atypical B cells. Among the CLL-like cells, the frequencies of follicular and marginal zone/marginal zone progenitor cells were reduced in Eμ-MTCP1 mice compared to wildtype littermates. Instead, atypical B cells lacking CD21 expression were substantially increased in diseased Eμ-MTCP1 mice. These CD19⁺/CD21⁻ cells exhibited populations with varying degrees of IgM and IgD expression, pointing toward some heterogeneity within the bulk tumor population. Overall, the malignant cells of Eμ-MTCP1 mice showed a CD19⁺/CD5⁺/

CD93⁻/B220^{dim} phenotype with dim surface expression of IgM, IgD, and CD23, confirming a B1a cell phenotype. With respect to these surface markers, a similar trend between Eμ-TCL1 mice and wildtype littermates was observed.

Eμ-MTCP1 leukemic cells are amenable to adoptive transfer in immunocompetent mice. Given the spontaneous B-cell leukemia in the Eμ-MTCP1 model resembled human CLL, the ability to adoptively transfer these cells into immune competent murine hosts would further provide rationale for promotion of this model as a pre-clinical research tool. On this basis, we engrafted splenocytes isolated from an Eμ-MTCP1 mouse having reached euthanasia criteria due to progressive CLL-like expansion into 10 C57/BL6NTac mice (Fig. 4A). Successful engraftment into the immune competent hosts was evident by 3–10 weeks. Left to proliferate without pharmacologic intervention, engrafted mice succumbed to the progressive leukemic accumulation between 5 and 18 weeks post-adoptive transfer (Fig. 4B–D). Splenomegaly was always apparent, accompanied by abdominal lymphadenopathy. Histopathologic analysis showed development of a systemic lymphoid neoplasia comprising homogenous, small-to-intermediate lymphocytes affecting the spleen, lymph nodes, liver,

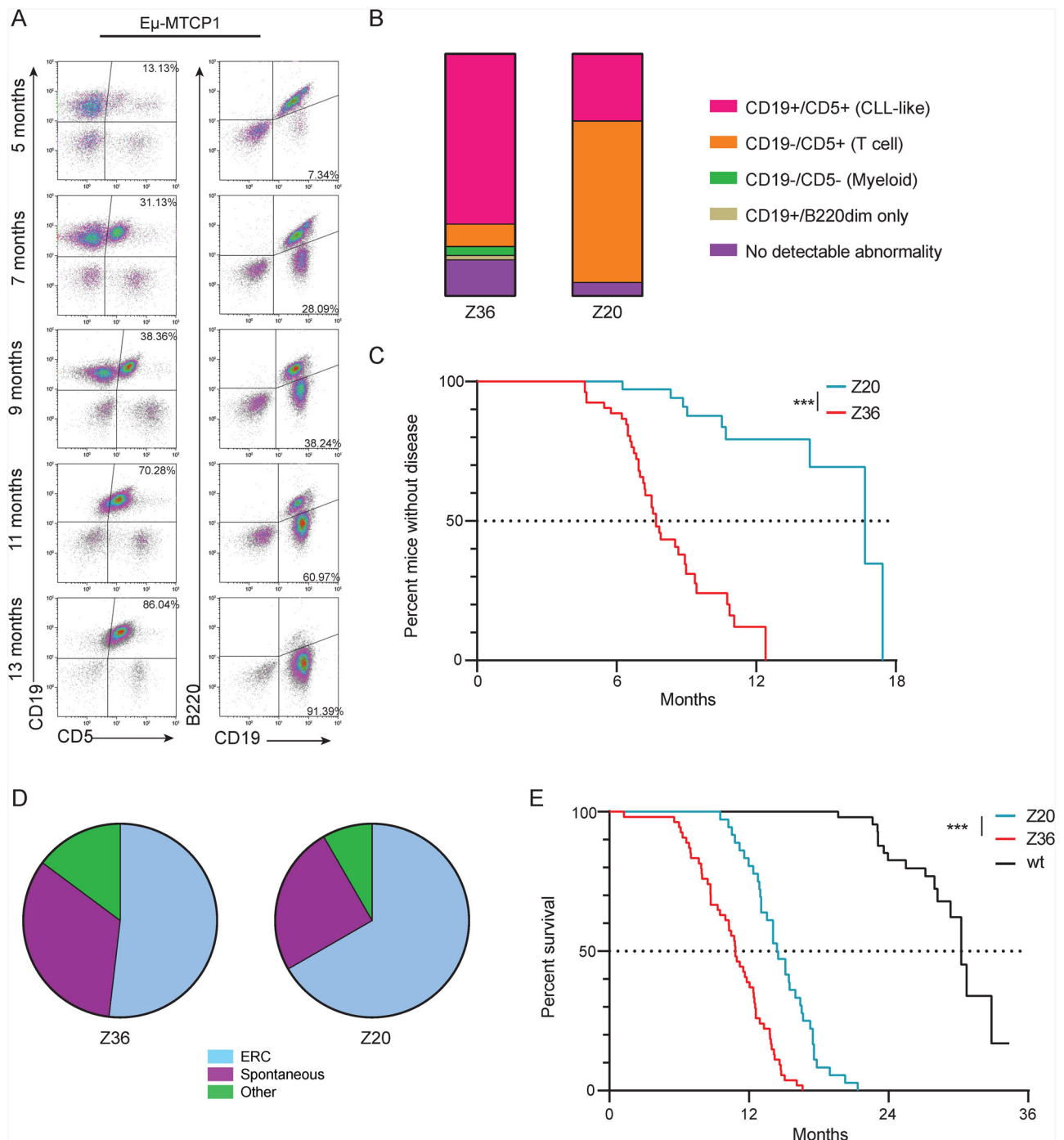


Fig. 2 Overexpression of *MTCP1* drives a lethal CLL-like leukemia. **A** Longitudinal flow cytometry analysis of a representative $E\mu$ -MTCP1 mouse showing progressive development of a CD45⁺/CD5⁺/CD19⁺ and CD19⁺/B220^{dim} CLL-like population in the blood. **B** $E\mu$ -MTCP1 mice (Z36, $n = 54$; Z20, $n = 36$) were followed monthly by flow cytometry for disease progression as described in **(A)**. Varying ratios of hemopathies were observed, including expansion of CD5⁺/CD19⁺ (CLL-like, pink) cells, CD5⁺/CD19⁻ cells (T cells, orange), CD5⁻/CD19⁻ (myeloid, green) cells, or CD19⁺/B220^{dim} only CLL-like cells (tan). **C** Kaplan-Meier estimation of median time to disease onset in $E\mu$ -MTCP1 mice (Z36 - red, $n = 54$; Z20 - blue, $n = 36$). Disease onset was defined as detection of >20% CD5⁺/CD19⁺ and CD19⁺/B220^{dim} CD45⁺ cells in the blood determined by flow cytometry. Median time from birth to disease onset was shorter in $E\mu$ -MTCP1 mice from the Z36 founder line (7.7 months) than from the Z20 line (16.7 months; $p < 0.001$). **D** Pie chart illustrating cause of death for $E\mu$ -MTCP1 mice (Z36, $n = 54$; Z20, $n = 36$). Cause of death for a majority of $E\mu$ -MTCP1 mice can be attributed to lethal progression of their disease burden. “ERC” = blue, mice met predefined early removal criteria. “Spontaneous” = purple, mice displayed disease progression identified by flow cytometry but had a spontaneous and unpredictable death. “Other” = green, mice died without measurable disease. **E** Kaplan-Meier estimation of median survival in $E\mu$ -MTCP1 mice (Z36 - red, $n = 54$; Z20 - blue, $n = 36$). The median survival time was 10.8 months (95% CI: 9.5-12) for $E\mu$ -MTCP1 founder line Z36 and 14.5 months (95% CI: 13.1-16) for founder line Z20 ($p < 0.001$). Representative survival of wildtype mice (black, $n = 54$) is shown as reference. *P* values (in **C** and **E**) determined by estimates from a Cox proportional hazards model.

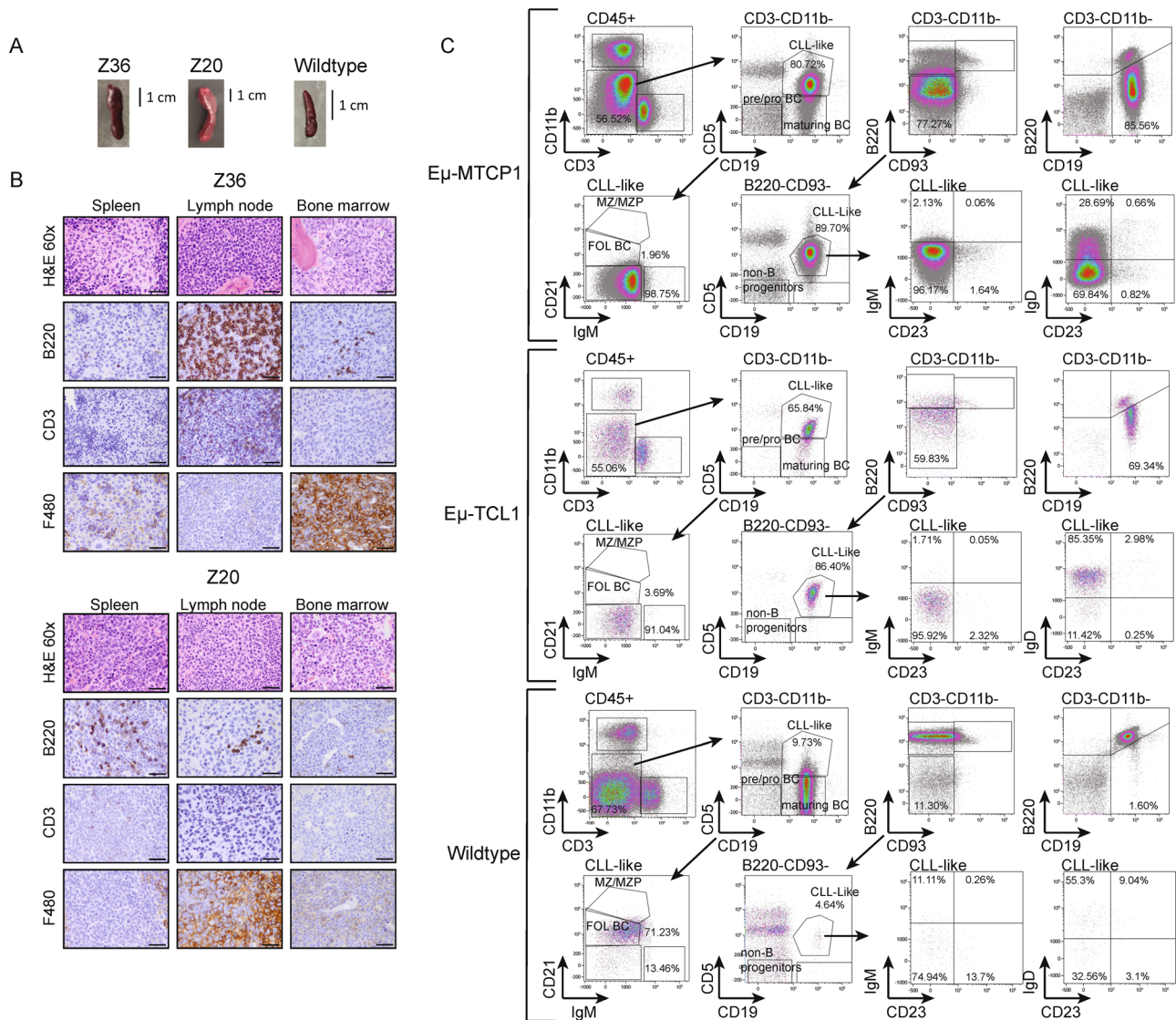


Fig. 3 Accumulation of abnormal B lymphocytes in $E\mu$ -MTCP1 mice. **A** Representative gross images of severely enlarged spleens from Z36 and Z20 founder $E\mu$ -MTCP1 mice, an observation consistently observed in subsequent progeny comprising the $E\mu$ -MTCP1 colonies. A representative gross image of a healthy spleen from an age-matched wildtype mouse is shown for comparison. Scale bar is 1 cm. **B** Post-mortem histopathology analysis of cervical lymph nodes, bone marrow, and spleen from $E\mu$ -MTCP1 founder mice Z36 and Z20 with CLL-like disease show histologic changes in multiple tissues consistent with a systemically disseminated mixed neoplasm containing B-lymphocytes and histiocytes. Lymphocytes were typically B220⁺, indicating a B-cell origin. CD3⁺ lymphocytes were sometimes scattered throughout the neoplasm and may be tumor infiltrating lymphocytes. Histiocytoid cells were identified as F4/80 positive in most cases. Cells null for B220, CD3, and F4/80 were occasionally observed. Z36 images representative of $n = 7$ evaluated mice, Z20 images representative of $n = 3$ evaluated mice. All organs visualized at 60x, scale bars are 33.3 μ m. **C** Representative immunophenotypic evaluation of B-cell populations in blood derived from $E\mu$ -MTCP1 (Z20 at ERC, 9 months old), $E\mu$ -TCL1 (at ERC, 12 months old) and wildtype mice (12 month old). CD3⁺ T and CD11b⁺ myeloid cells were gated out and cells were plotted using CD19 and CD5 expression markers to identify CD19⁺CD5⁺ population (CLL-like cells) and CD19⁺CD5⁻ (maturing B cells). CD19⁺CD5⁺ population were further dissected according to CD21 and IgM expression to identify CD21⁺IgM⁺ marginal zone/marginal zone progenitor (MZ/MZP) B cells, CD21^{int}IgM^{dim} follicular B cells, CD21⁻IgM⁻ and CD21⁻IgM⁺ atypical B cells. CLL-like cells were also evaluated for IgD and CD23 expression. Overall, the malignant cells of $E\mu$ -MTCP1 mice showed a CD19⁺CD5⁺CD93⁻B220^{dim} phenotype with dim surface expression of IgM, IgD, and CD23 confirming a B1a cell phenotype.

bone marrow, Peyer’s patches, thymus, serosal surfaces of viscera; and rarely, lung and kidney (Fig. 4E). Thus, while a mixed lineage neoplasia was observed in $E\mu$ -MTCP1 founder lines with a CLL-like leukemia, only the B-lymphoid portions of the total leukemic burden successfully engrafted and continued to proliferate in the host.

CLL-like transcriptional profile identified in CD19⁺CD5⁺ populations from $E\mu$ -MTCP1 mice. To understand if the

aggressive murine leukemia in $E\mu$ -MTCP1 transgenic mice were composed of heterogeneous, polyclonal B cells or derived from a single precursor founding a homogeneous tumor population as is the case in human CLL, we evaluated the B-cell receptor (BCR) repertoire by examining *IGH* transcripts via RNA-sequencing methods previously described by our group³⁶. Prominent usage of distinct heavy chain gene loci representing a clonal B cell expansion was observed from splenic B cells isolated from 3/3 $E\mu$ -MTCP1 mice and similarly in 3/3 $E\mu$ -TCL1 mice, a stark contrast from the high degree of clonal variability exhibited in wildtype

mice (Fig. 5A, Supplementary Table 3). The major clone in 2/3 E μ -MTCP1 and 3/3 E μ -TCL1 mice predominantly used V_{H1} and V_{H12} family genes, while 3/3 wildtype mice predominantly used V_{H5} family genes. One analyzed E μ -MTCP1 mouse used V_{H5} family genes in its dominant clones. The V_{H12}-3 gene was shared as that predominantly used in the major clone of one E μ -MTCP1 and E μ -TCL1 mouse. The most abundant tumorigenic clones isolated from E μ -MTCP1 spleens exhibited a low *IGHV* mutational burden (Supplementary Fig. 4A), well below the threshold for classification³⁷ as “mutated” (Supplementary Fig. 4B). The low mutational burden in this region is consistent with the aggressive, *IGHV*-unmutated, subtype of human CLL.

We next sought to determine the overall transcriptional profile of these monoclonal tumor cells. Principal component analysis of global transcription profiles revealed significant segregation of splenic B-cells collected from E μ -MTCP1 and E μ -TCL1 mice, and splenic B-cells from wildtype littermates across PC1 (Fig. 5B). Further, a significant overlap in gene expression most variable from wildtype splenic B-cells was found when evaluating E μ -MTCP1 or E μ -TCL1 transgenic strains, suggesting the leukemic B1a cells in E μ -MTCP1 mice have achieved a transformed state by both phenotypic and transcriptomic standards (Fig. 5C, D). Ingenuity pathway analysis (IPA) of significantly enriched genes (Log2FC > 2, $p < 0.001$) shared between E μ -MTCP1 and E μ -TCL1 transgenic strains when compared to wildtype littermates primarily converged on genes involved in G protein-related signaling pathways (Supplementary Fig. 5A), likely a consequence from both MTCP1 and TCL1 acting as activators of AKT. In genes uniquely enriched in E μ -MTCP1 mice compared wildtype littermates, IPA analysis converged on FAK and PTEN signaling, Rho family GTPase signaling, and protein kinase A/cAMP-mediated signaling (Fig. 5E). Directly comparing E μ -MTCP1 and E μ -TCL1 mouse transcriptomes revealed a considerable degree of similarity, where only 79 of 15,318 analyzed genes displayed significant variation from one transgenic model to the other (Fig. 5F, Supplementary Fig. 5B). Specifically, 38 genes were identified as overrepresented in E μ -TCL1 mice, highlighted by the presence of various nucleotide binding factors (*Atrip*, *Ddx60*, *Trim6*), heat shock proteins (*Hspa1a/b*), and other known oncogenic markers (*Adm*, *Eef2k*, *Ili2a*, *Ly6i*, *Mapk8*, *Map3k20*, *Pmaip1*, *Wnt16*). Relative overexpression of 41 genes was noted in E μ -MTCP1 mice, marked by the presence of cell signaling molecules (*Ccr10*, *Lrp5*, *Zbtb4*) and other known oncogenic markers (*Cd34*, *Ptgs1*). Notably, no change in *Tcl1* transcript abundance was observed between E μ -MTCP1 and wildtype mice, and no change in *Mtcp1* transcript abundance was observed between E μ -TCL1 and wildtype mice (Supplementary Fig. 5C), suggesting the *TCL1*-driven murine leukemia acts independently from *MTCP1* and the *MTCP1*-driven murine leukemia acts independently from *TCL1*.

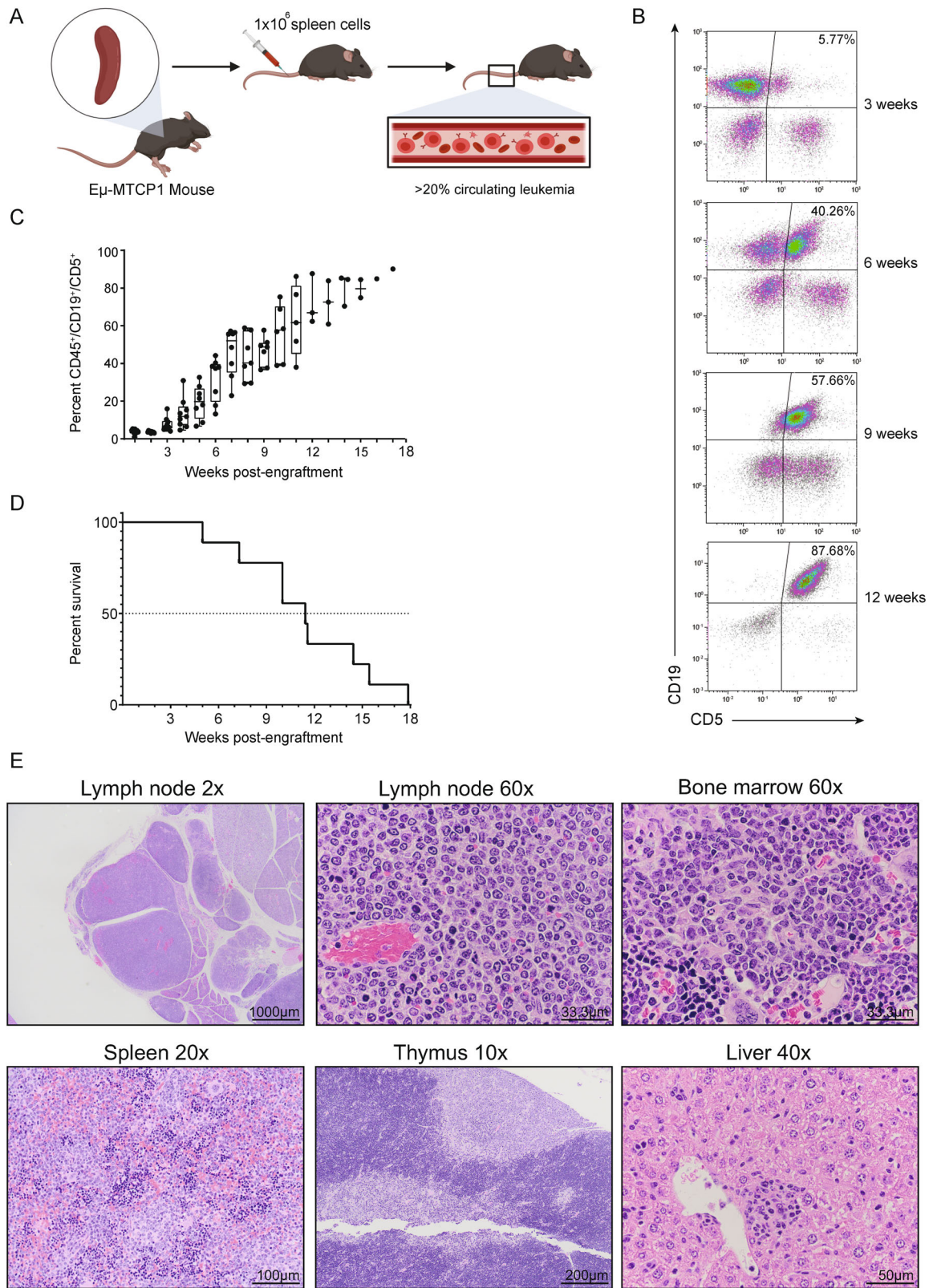
Ibrutinib treatment impairs E μ -MTCP1 leukemia development. We previously demonstrated the significance of constitutive activation of BCR signaling pathways in promoting proliferation of CLL cells, highlighting efficacy of the Bruton tyrosine kinase (BTK) inhibitor ibrutinib in abrogating leukemic advancement even in pre-leukemic stages³⁸. To evaluate the sensitivity of the MTCP1-driven murine leukemia to ibrutinib, E μ -MTCP1 pups from founder line Z36 were treated continuously from the time of weaning with drinking water containing ibrutinib at ~30 mg/kg/day or 10% cyclodextrin (vehicle). Monthly assessment of circulating CD5⁺/CD19⁺ and CD19⁺/B220^{dim} leukemia cells in all treated mice displayed a lower leukemic burden at 6 and 12 months, contributing to considerable survival prolongation in mice receiving ibrutinib at

12 months of age (Fig. 6A, B). We further evaluated the use of the E μ -MTCP1 adoptive transfer model for pre-clinical evaluation of CLL drug candidates. Successfully engrafted mice with comparable disease load (percent CD19⁺/CD5⁺ B cells in the blood) were randomly assigned to receive ibrutinib or vehicle by daily oral gavage at any given enrollment time to control for different growth kinetics of the engrafted tumor cells. Similarly, ibrutinib administration led to a reduction in the rate of disease development between six and 12 weeks post-enrollment and prolonged survival compared to those receiving vehicle (Fig. 6C, D). Post-mortem histopathology analysis supported these evaluations, where ibrutinib-treated mice displayed less-severe organ involvement (Fig. 6E).

Discussion

Here, we identified an index CLL patient bearing an uncommon, reciprocal t(X;14)(q28;q32) translocation joining the *MTCP1* locus with immunoglobulin heavy chain regulatory elements (*IGH*; 14q32), an event analogous to the *IGH* translocations with *MYC*, *CCND1*, or *BCL2* genes driving various B-lymphomas^{39,40}. After observing that this translocation occurs in CLL, we further discovered that even without an Xq28 rearrangement *MTCP1* mRNA is overexpressed in CLL cells as compared to normal B-cells. The observed overexpression of *MTCP1* in CLL and the discovery of a translocation that juxtaposes with the *IGH* locus suggest a pathogenically relevant role of *MTCP1* in CLL. Notably, increased *MTCP1* expression in this CLL cohort lacked major correlation with pre-treatment characteristics but was associated with a shorter response to chemoimmunotherapy. This relationship may reflect the current understanding of *TCL1* expression in CLL, where inter-patient variability remains the norm yet patients with the lowest *TCL1* expression maintain favorable outcomes following chemoimmunotherapy^{41,42}. Further correlating *MTCP1* expression with PFS, a bivariate analysis identified a 2-fold increase in *MTCP1* expression as a prognostic indicator of PFS independent of *IgHV* status, a known high-risk factor in CLL. Importantly, however, *IgHV* mutation status as a single variable was not prognostic for reduced PFS in this chemoimmunotherapy cohort—which is atypical in CLL—suggesting further large scale correlative studies are necessary to provide a comprehensive assessment of the associations between higher *MTCP1* expression and other high-risk factors in CLL.

In a multivariate analysis, a 2-fold increase in *MTCP1* expression lost strong association with reduced PFS while adjusting for additional predictors for reduced PFS in these chemoimmunotherapy trials (Zap-70 methylation, high-risk cytogenetics, sex, WBC). This result implicates *MTCP1* as a factor with considerable influence on the CLL disease course; yet it may not act as the fundamental driving element, which is not entirely surprising considering the abundance of evidence conferring the significant relationship between CLL outcomes and these other high-risk factors. Even so, revealing mechanisms supporting *MTCP1* upregulation in CLL may provide meaningful insight to the overall pathogenesis of this disease. Similar to studies evaluating *TCL1* in CLL^{43–45}, the apparent inter-patient variability suggests multiple factors likely contribute to dysregulation of *MTCP1* expression; where loss of microRNA-mediated negative regulation or *MTCP1* upregulation via stimulating signals from the tumor microenvironment are primary candidates for further evaluation. Likewise, exploring BCR-induced kinase cascades, with particular attention given toward the role for PKC- β ⁴⁶, may facilitate understanding of the upstream mechanisms upregulating and activating *MTCP1* in CLL. Other mechanisms supporting *MTCP1* upregulation, such as loss of epigenetic control or evasion of X chromosome inactivation (although we



observed an even male:female distribution between *MTCP1* expression quartiles) serve as additional unexplored means facilitating *MTCP1* upregulation in CLL. In addition, exploration of this gene in other diseases such as acute myeloid leukemia (AML) might be considered based upon the recent identification of a t(X;17)(q28;q21) rearrangement resulting in a *KANSL1-MTCP1* fusion gene in an AML patient⁴⁷.

Supporting the notion that *MTCP1* expression beyond basal levels is advantageous for leukemogenic B cells, screening a large cohort of suspected CLL cases revealed seven additional Xq28 rearrangements with unexplored relevance; two with a translocation at the 12q32 site, one each involving 8q22 or 8q24.2 sites, and three joining unrecognized material with the Xq28 site. Microdeletions in the 12q32 site including the *HOXC* cluster and

Fig. 4 The CLL-like disease populating the spleen of E μ -MTCPI mice is amenable to adoptive transfer. **A Schematic review of E μ -MTCPI adoptive transfer leukemia model. 1×10^6 splenocytes isolated from an E μ -MTCPI mouse (from founder line Z36) having reached predefined euthanasia criteria due to progressive leukemic expansion were engrafted via tail vein injection into immunocompetent C57/BL6NTac (wildtype) mice. **B** Immunocompetent recipient mice described in **(A)** were monitored weekly for expansion of CD5⁺/CD19⁺ and CD19⁺/B220^{dim} circulating CD45⁺ cells by flow cytometry. A representative flow analysis is shown describing the progressive accumulation of CD45⁺/CD5⁺/CD19⁺ cells. **C** Nine of ten recipient mice displayed significant peripheral disease (CD45⁺/CD5⁺/CD19⁺ cells) between 3 and 10 weeks post-adoptive transfer of splenic cells from E μ -MTCPI mice. In mice surviving at least 12 weeks post-engraftment, the engrafted tumor population nearly composes the entire peripheral blood compartment (>75%). Box elements reflect 2nd - 3rd quartile, center line reflects the median value, and whiskers reflect the distance from the upper and lower limit to the box elements. **D** Kaplan–Meier estimation of median survival in recipient adoptive transfer mice. Without intervention, adoptive transfer of splenic CLL-like cells from E μ -MTCPI mice results in a lethal disease with a median time to disease at 11.4 weeks. All successfully engrafted mice eventually succumbed to disease. **E** Representative post-mortem histopathology analysis of lymph node (2x, 60x), bone marrow (60x), spleen (20x), thymus (10x), and liver (40x) from a mouse in the E μ -MTCPI adoptive transfer model reaching ERC due to progressive disease. Hematoxylin & eosin staining shows histologic changes consistent with a systemically disseminated round cell neoplasm of small to intermediate lymphocytes that was homogenous between engrafted animals. Images representative of $n = 3$ mice. Scale bars as indicated.**

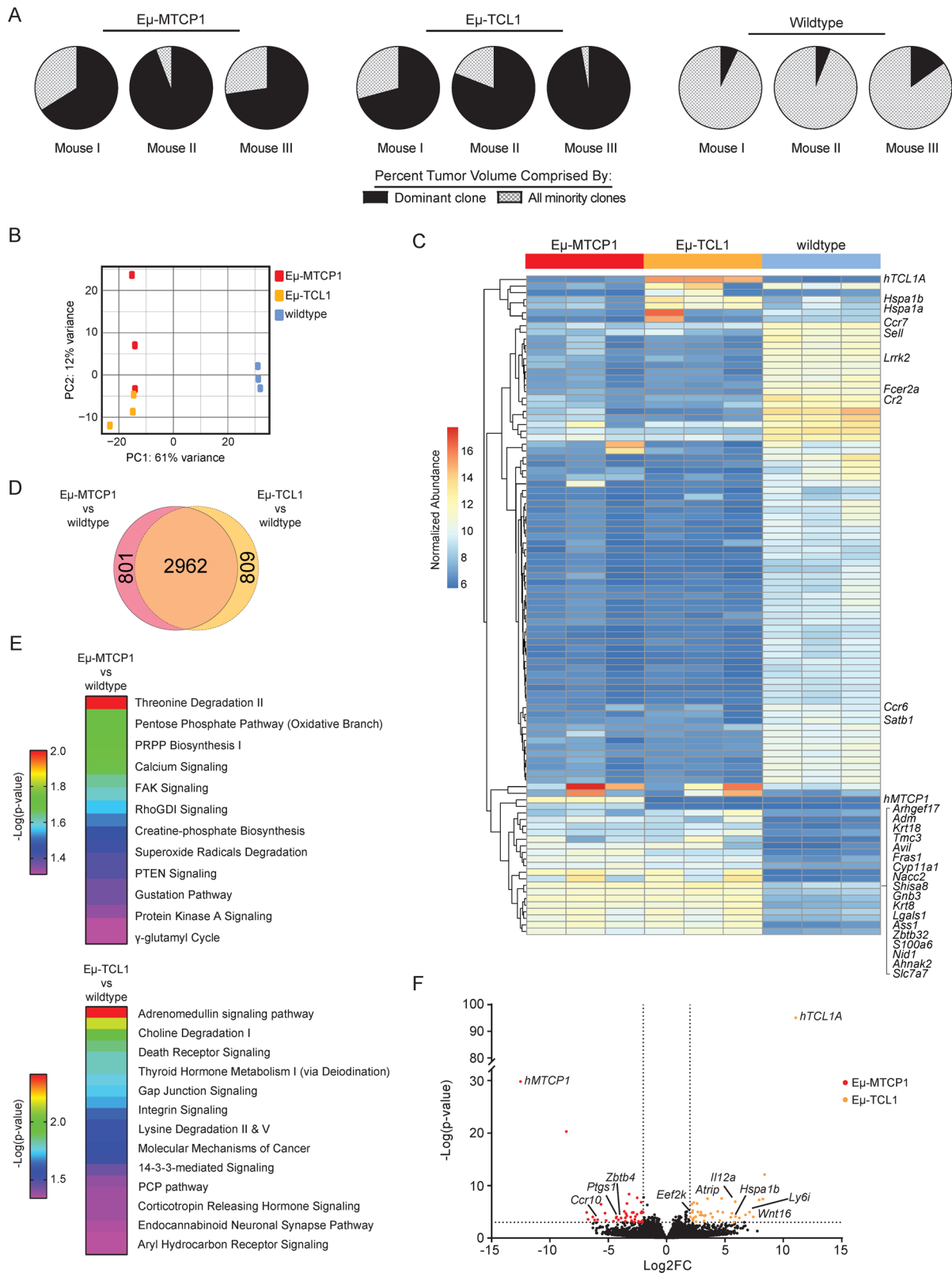
other adjacent genes results in significant disruption of normal cell function^{48–50}, and amplification of the 8q22 site including *EDD1* and *GRHL2* genes, negative regulators of apoptosis, have been described in breast, pancreas, and lung cancer cells as a mechanism for evasion of death receptor-activated therapies⁵¹. The 8q24.2 region is a gene desert containing *MYC* enhancer elements and variations at this site are known to influence CLL⁵². Interestingly, the t(X;8)(q28;q24.2) case reported here was identified in a patient screened initially on the basis of suspected CLL which was later found to be DLBCL. Cytogenetic evaluation of this patient, a 59 y/o male, also identified a t(3;9)(q27;q32) rearrangement involving the *BCL6* gene and a t(14;19)(q32.3;q13.2) rearrangement involving the *BCL3* gene. This t(14;19) rearrangement, joining the *BCL3* locus with *IGH* elements, occurs in DLBCL and other chronic lymphoproliferative disorders but is most frequently observed in CLL. However, t(14;19) CLL cases are often atypical with distinctive clinicopathologic and genetic features including younger age, aggressive clinical course, and association with trisomy 12, which was also present in this patient^{53,54}. Translocation of the *MTCPI* locus under *MYC* enhancer elements in this unusual case supports our finding that, while rare, genomic rearrangement events resulting in up-regulation of the *MTCPI* gene may contribute to the transformative potential of the leukemic B cell and influence the overall trajectory of the resulting tumor burden. Juxtaposition of the *MTCPI* gene locus with these additional sites is of considerable interest and further investigation will be required to fully describe their significance.

To establish a definitive role for *MTCPI* as a pathogenic contributor in CLL, we generated a mouse model with B cell-specific overexpression of human recombinant *MTCPI* (E μ -MTCPI). Longitudinal evaluation of E μ -MTCPI littermates revealed a majority of these mice developed a lethal hematologic malignancy, highlighted by the progressive emergence of CLL-like B cells or hyperproliferative T cells circulating in the blood and accumulating in the spleen and lymph nodes. The CLL-like population in E μ -MTCPI mice bears a striking resemblance to the disease that develops in E μ -TCL1 mice; however, the timeline for clinical deterioration from CLL-onset to death was accelerated in both E μ -MTCPI founder strains. The observed disparity in median estimated survival between E μ -MTCPI founder strains Z20 and Z36 appears to be largely driven by the delayed rate of leukemia onset in Z20 lineage mice. While we confirmed >10 copies of the *MTCPI* transgene were inserted in both founder lines, we acknowledge the integration site occurred at two distinct locations on different chromosomes for each respective founder. While mechanisms supporting the observed variance in leukemia onset between Z20 and Z36 founder lines remain unresolved,

insertion of the *MTCPI* transgene in proximity to additional active enhancer regions or inaccessible in regions of condensed chromatin may be contributing to this distinction. Shared between founder lines, however, the cause of death for a majority of E μ -MTCPI mice was attributed to disruption of critical organ function due to systemic malignant infiltration comprised primarily of mixed populations of small-to-intermediate-sized lymphocytes and larger histiocytoid cells. Similar to what is often observed in CLL patients, the spleens of E μ -MTCPI mice were deformed, consistently presenting with substantial splenomegaly.

Further analysis of B lymphocytes from E μ -MTCPI mice revealed that this CLL-like disease may present a faithful resemblance to human CLL. We found that circulating CLL cells from E μ -MTCPI mice had intracellular, but lacked surface expression of the immunomodulatory molecule CTLA4, consistent with human CLL cells but not E μ -TCL1 CLL-like cells³⁴. Immunophenotypic analysis of the CD19⁺/CD5⁺ cells of E μ -MTCPI mice revealed the vast majority were B220^{low}/CD93[–] expressing cells, suggesting a B1a cell phenotype. Scant numbers of IgM⁺ or IgD⁺ were found within this population, corroborating histopathology reports suggesting some degree of heterogeneity is evident within the malignant population. Engraftment of bulk splenocytes from E μ -MTCPI mice with CLL-like disease into immune competent hosts resulted in a homogeneous expansion of tumorigenic B lymphocytes, suggesting the true tumor population is comprised of the clonally related B1a cells and the chronic inflammatory milieu produced by the proliferating B-cells in E μ -MTCPI mice may promote proliferation of macrophages, plasma cells, and extramedullary hematopoiesis.

Having demonstrated that the E μ -MTCPI mouse model generates a CD19⁺/CD5⁺ B-cell malignancy with resemblance to human CLL, we proposed that this model may be ideally suited for pre-clinical evaluation of therapeutic agents for consideration in CLL and related diseases. To support this proposal, we demonstrated that continuous ibrutinib administration in pre-leukemic mice delayed disease onset and prolonged survival. In an adoptive transfer model, daily ibrutinib dosing delayed the rapid advancement of engrafted E μ -MTCPI splenocytes and resulted in a dramatic prolongation in survival. The moderate reduction in circulating lymphocytes upon treatment with ibrutinib in this adoptive transfer model is consistent with the understanding that inhibition of BCR signaling via ibrutinib drives cell mobilization from nodal sites and often results in prolonged lymphocytosis⁵⁵. The dramatic prolongation in survival seen here is likely a result of less severe occupation of proliferative lymphoid compartments and defacement of normal organ architecture in engrafted mice. Overall, the observed



response to inhibition of BCR signaling encourages further use of this model in development of novel derivatives with varying specificity for BTK and other components of the BCR pathway.

Although the overall transcriptome profile remained largely similar between Eμ-MTCP1 and Eμ-TCL1 tumor cells, further investigation to define the significance in variation between MTCP1- and TCL1-driven CLL is warranted. Specifically,

elucidating the leukemogenic mechanisms which ultimately led to an accelerated disease course from CLL-onset to death in Eμ-MTCP1 mice is of considerable interest but is beyond the scope of the present study. Furthermore, the conserved structure between MTCP1 and TCL1A proteins and similarities in the resulting murine and human CLL phenotype suggest shared activation of AKT and other leukemogenic pathways; pathways which may be

Fig. 5 Transcriptome profiling reveals transformed B cells in Eμ-MTCP1 mice. **A** Comparison of *IGHV* gene usage among Eμ-MTCP1 (founder Z36), Eμ-TCL1, and wildtype mice ($n = 3$ per group) demonstrated clonal tumor populations in Eμ-MTCP1 and Eμ-TCL1 mice. Visualized via pie chart, the percent tumor volume comprised by the dominant clone of each mouse shown in black. All minority clones are grouped and their percent contribution is visualized via gray-checked pattern. Gene names of the top 10 *IGH* genes in order of abundance are presented in Supplementary Table S3. **B** Unbiased RNA-sequencing of splenic B-cells isolated from Eμ-MTCP1 (founder Z36), Eμ-TCL1, and wildtype mice ($n = 3$ per group) revealed distinct clustering of Eμ-MTCP1 (red) and Eμ-TCL1 (yellow) samples from wildtype mice (blue) as visualized by principle component analysis. 62% variance was observed along PC1, and 12% variance was observed along PC2. **C** The 100 most-variable genes from (B) visualized via heatmap. A majority of these significantly differing genes encode *IGH* genes (not shown for clarity—whole list of genes can be found in the source data). Genes listed on the y axis are arranged via hierarchical clustering using Euclidean distance measurements. Heat map scale is representative of normalized Log2 expression between all samples. **D** Euler diagram visualizing differentially expressed genes between Eμ-MTCP1 vs wildtype mice (left circle, pink) and Eμ-TCL1 vs wildtype mice (right circle, yellow). A significant overlap (2962/4572; 65%) in the number of differentially expressed genes compared to wildtype mice were shared between Eμ-MTCP1 and Eμ-TCL1 mice (middle overlap, orange). **E** Ingenuity pathway analysis (IPA) of significantly enriched genes ($\text{Log}_2\text{FC} > 2$, $p < 0.001$) unique to Eμ-MTCP1 vs wildtype mice or Eμ-TCL1 vs wildtype mice. Rainbow color scale reflects $-\text{Log}(p \text{ value})$ determined via Fisher's exact test. Complete list of IPA terms and p values are available in the Supplementary File: source data. **F** Differential mRNA expression analysis of splenic B cells from Eμ-MTCP1 and Eμ-TCL1 mice visualized via volcano plot ($n = 3$ per group). Seventy-nine genes enriched in Eμ-MTCP1 mice (red) or Eμ-TCL1 mice (yellow) are shown ($\text{Log}_2\text{FC} > 2$; $p < 0.001$). P value determined in DESeq2 via Wald test. Complete list of genes and p values are available in the Supplementary File: source data.

independently activated as no observable change in *Tcl1* expression was found in Eμ-MTCP1 mice and no observable change *Mtcp1* expression was found in Eμ-TCL1 mice. Validation of this relationship remains unreported, however, for which the Eμ-MTCP1 mouse presents an excellent tool to study these mechanisms. The transgenic strategy of the Eμ-MTCP1 mouse presented herein also supports the notion that the *CMC4* gene is merely a passenger in the t(X;14)(q28;q32) rearrangement and may not provide an essential role in the leukemogenic transforming event. Regardless, *CMC4* expression was indeed elevated in CLL cells when compared to normal B-cell subsets. When translated to the short p8 MTCP1 isoform this protein is localized to the mitochondria⁵⁶, likely suggesting an indirect role in supporting leukemogenesis via metabolic pathways. Thus, complete investigation of the relationship between p8 and p13 MTCP1 may further define the collective oncogenic impact of Xq28 rearrangements.

A broader and more general finding relevant to other types of cancer is the successful application of a strategy pursuing the functional consequence of genes involved in rare chromosomal abnormalities. Exploring the rare t(14;18)(q32;q21) translocation in CLL, such approaches facilitated understanding of the significance of the anti-apoptotic protein *BCL2* and *miR-15/16* at the minimal deleted region of del(13q14)^{12–14}. These microRNAs contribute to the pathogenesis of CLL, and *BCL2* represents an exceptionally valuable therapeutic target¹⁵. Whole genome sequencing may effectively identify translocations involving *BCL2* and *IGH*⁵⁷, but the t(X;14)(q28;q32) rearrangement has not been previously reported. This and other Xq28 translocations may have escaped notice for several reasons. Identification of non-fusion gene translocations [i.e., precisely the situation in t(v;14)(v;q32) translocations] may be hampered by fundamental limitations of short-read sequencing, namely poor mappability of highly repetitive regions flanking translocation breakpoints. In addition, the infrequent occurrence of these Xq28 changes in the very large cytogenetics cohort in our series—as compared to the largest WGS study of CLL⁵⁷ is another potential explanation. Regardless, our experience suggests an opportunity for both classic cytogenetics and WGS assessment of rare recurrent balanced translocations to provide an avenue in other cancers to identify previously unrecognized oncogenes.

In summary, evidence from both human CLL and a transgenic mouse model present a causal relationship between *MTCP1* and CLL. The Eμ-MTCP1 mouse model should be considered as an alternative tool for both biologic assessment of co-expressed

genes and pre-clinical evaluation of CLL therapeutics. Identification of *MTCP1* as a significant factor in the pathogenesis of CLL provides an additional molecular target for consideration in this disease, and an archetypical process for the future pursuit of rare balanced translocations for the identification of genes relevant to pathogenesis and progression in many cancers.

Methods

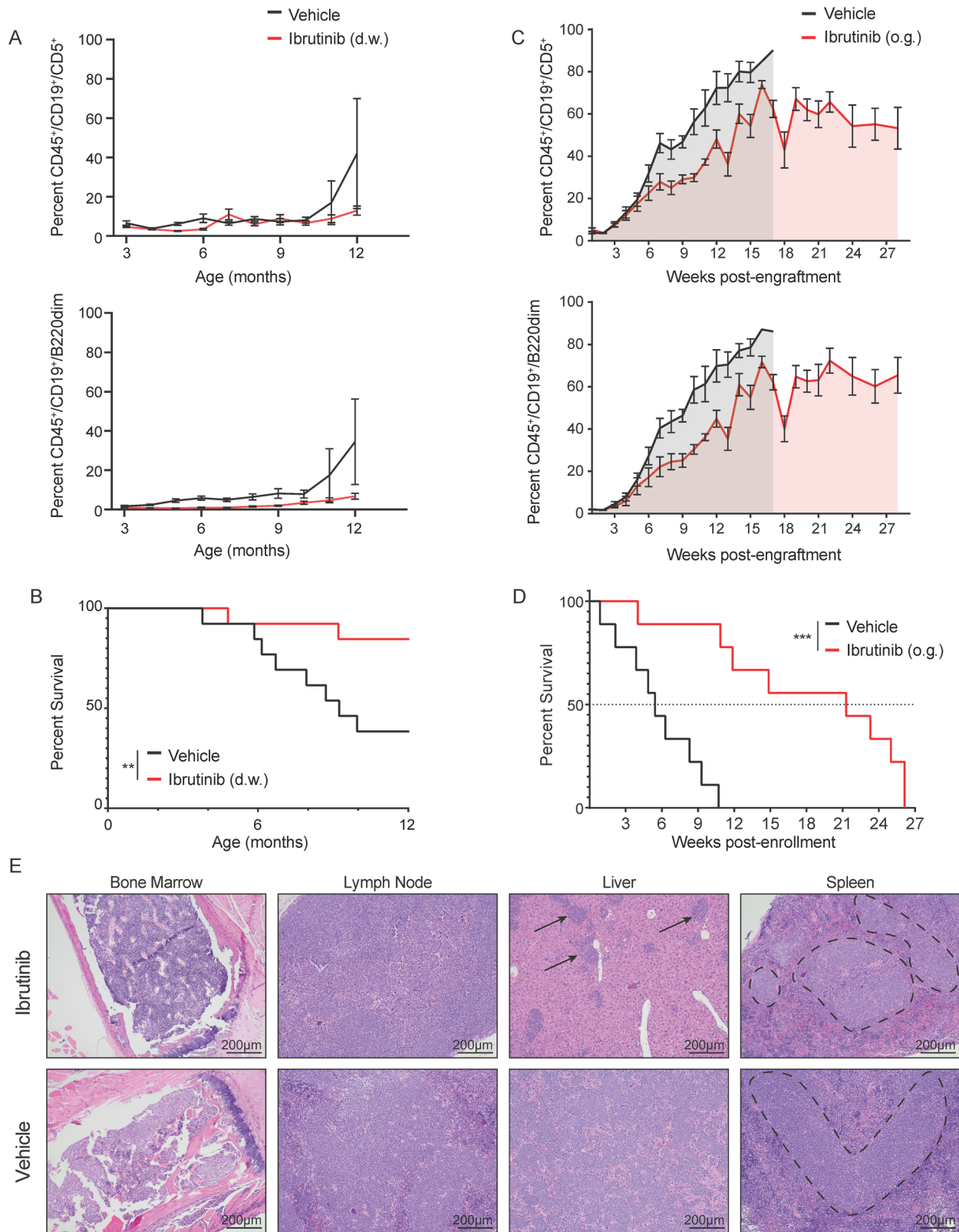
Screening suspected CLL cases for Xq28 rearrangements. A total of 1744 suspected CLL specimens collected between November 2003 and December 2014 at The Ohio State University Comprehensive Cancer Center were evaluated for possible Xq28 rearrangements by screening metaphase karyotypes collected at time of initial biopsy. Translocations involving Xq28 were confirmed by two independent cytogeneticists.

MTCP1 and *CMC4* gene sequences were obtained and visualized from the Ensembl genome browser. The proposed 3-dimensional crystal structure for *MTCP1* and *TCL1A* protein sequences were obtained from the RCSB Protein Data Bank (IDs: 1A1X, 1JSG, respectively)^{18,19}. Crystal structures were determined via X-ray diffraction and presented at 2.00 Å and 2.50 Å resolution, respectively. Gene expression data for *MTCP1* and *CMC4* determined from RNA-sequencing were collected from the Blueprint DCC data portal⁵⁸. For evaluation of *MTCP1* expression via RNA-sequencing, de-identified human CLL cells were isolated as previously described after obtaining informed consent on protocols approved by The Ohio State University Cancer Institutional Review Board.

Fluorescent in-situ Hybridization. Fluorescent in-situ Hybridization (FISH) was performed with *IGH/CCND1* XT, *IGH* break apart (Abbott Molecular, Downers Grove, IL) and *MTCP1* (Empire Genomics, Williamsville, NY) probes. FISH was done according to the manufacturer's recommendations, except prior to hybridization slides were pretreated with pepsin and postfix solution. Co-denaturation of probe and sample was done on HyBrite (Abbott Molecular, Downers Grove, IL) for 5 min at 73 C. Hybridization was carried out overnight at 37 C, and slides were washed in 0.4 x SSC/0.3%NP-40 for 2 min at 73 C. The signals were viewed using a fluorescent microscope (Zeiss AxioScope 40) equipped with appropriate filters and analyzed with Applied Imaging System.

Generation of the Eμ-MTCP1 mouse model. Transgenic Eμ-MTCP1 mice were generated on a C57BL/6NTac background at The Ohio State University Comprehensive Cancer Center's Transgenic Mouse Facility via pronuclear injection of linear constructs derived from a plasmid vector encoding murine immunoglobulin mu enhancer elements followed by human cDNA encoding the p13 kDa *MTCP1* protein. An equal ratio of male and female mice were maintained throughout all analyses.

From five unique transgenic founder lines, detailed characterization was conducted in two lines showing early evidence of a disease phenotype (Z36 & Z20). Genotyping of Eμ-MTCP1 progeny was performed using the following *MTCP1* primer sequences: (forward: 5' ATCTGCCGCCACCATGGC 3'; reverse: 5' GCTTAAGCAACAGCTCCTGTAC 3'). All experiments were carried out under protocols approved by The Ohio State University Institutional Animal Care and Use Committee. Pre-defined euthanasia criteria for mice in all transgenic colonies and murine transplant models included lethargy, impaired motility, splenomegaly, enlarged lymph nodes, decrease in body weight (>20%), development of tumor masses, ruffled fur, hunched back, failure to nest, and loss of appetite. All veterinary



technicians determining removal criteria were blinded to transgenic strain and treatment group.

Transgenic mouse mapping and gene integration services were provided by Taconic Biosciences via a collaboration between Taconic and Cergentis. Sample preparation was carried out at Taconic Biosciences and both TLA and data analysis were carried out at Cergentis as described previously³⁰, with genotyping assay recommendations subsequently provided by Taconic. The *MTCP1* transgene

integrated at chr8:58,833,688–58,838,745 in an intron of the *Galnt6* gene (Founder Line Z20). The region in the genome between the 5' and 3' integration site was deleted during the integration event. No structural variations were detected in the transgenic sequence of this sample and >10 copies of the transgene have integrated in this locus. Similarly, the *MTCP1* transgene integrated at chr7:100,715,866–100,720,642 within an intron of the *Fam168a* gene (Founder line Z36). The genomic region between the 5' and 3' integration site was deleted during

Fig. 6 MTCPI-driven murine leukemia is responsive to BTK inhibition. **A** Continuous BTK inhibition via ibrutinib delays progression of a spontaneous leukemia in E μ -MTCPI mice most evident by 12 months of age (CD19⁺/CD5⁺, $p = 0.018$; CD19⁺/B220^{dim}, $p = 0.012$ determined via Cox proportional hazards model). E μ -MTCPI mice ($n = 13$ per group) began continuous dosing of ibrutinib (~30 mg/kg/day, red line) or vehicle (10% cyclodextrin, black line) via drinking water (d.w.) beginning at two months of age. Plot reflects mean \pm SE. **B** Mice from (**A**) were followed, revealing continuous BTK inhibition via ibrutinib (red line) prolongs survival compared to vehicle (black line, $p = 0.006$). **** represents estimation from a Cox proportional hazards model. **C** Adoptive transfer of 1×10^6 splenic E μ -MTCPI CLL-like cells via tail vein to immune competent wildtype host mice results in a progressive leukemic expansion that is delayed upon treatment with ibrutinib. Mice were enrolled to receive either ibrutinib (red line, 25 mg/kg; $n = 9$) or vehicle (black line, 0.5% methylcellulose/1% Tween80; $n = 9$) via daily (Mon-Fri) oral gavage (o.g.) upon reaching >20% CD5⁺/CD19⁺ and CD19⁺/B220^{dim} CD45⁺ cells in the blood. Ibrutinib administration delayed the rate of leukemic progression measured at six ($p = 0.063$) and 12 weeks ($p < 0.001$) post-engraftment. P values determined via mixed effects model. Plot reflects mean \pm SE. **D** Median survival time for mice in (**C**) is significantly extended upon daily administration of oral ibrutinib (red line, median survival = 28.4 weeks), extending well beyond the median survival observed with vehicle treatment (black line, median survival = 11.4 weeks; $p < 0.001$). ***** represents estimation from a Cox proportional hazards model. **E** Post-mortem histopathology analysis of organs and tissues from mice in (**C**) receiving either ibrutinib (top panel) or vehicle (bottom panel) having succumbed to disease. Hematoxylin & eosin staining reveals extensive neoplastic infiltrates effacing the bone marrow and lymph nodes in both ibrutinib and vehicle treated mice, while infiltrates are less severe in the liver and spleen of mice treated with ibrutinib. Neoplastic cells are observed as discrete, basophilic nodules in the livers (arrows) and spleens (circled regions) of the ibrutinib-treated mice, whereas in the vehicle-treated mice, neoplastic cells tended to form diffuse sheets or larger/confluent nodules. All organs visualized at 10x, scale bars are 200 μ m.

the integration event. No structural variations were detected in the transgenic sequence, and >10 copies of the transgene have integrated in this locus.

Immunophenotyping. Due to the high concordance between spleen and lymph nodes, immunophenotyping results are depicted for the spleen. Immunophenotyping of tumor cells in peripheral blood, spleen, and lymph node of E μ -MTCPI and E μ -TCL1 mice by flow cytometry was performed as follows: APC rat anti-mouse CD45 (1/100 dilution; BD Biosciences Cat #559864), FITC rat anti-mouse CD45R/B220 (1/50 dilution; BD Biosciences Cat #553088), BV421 rat anti-mouse CD19 (1/50 dilution; BD Biosciences Cat #562701), PE rat anti-mouse CD5 (1/100 dilution; BD Biosciences Cat #553023). Immunomodulatory assessment of E μ -MTCPI peripheral blood by flow cytometry was performed as follows: PE hamster anti-mouse CTLA4 (1/16 dilution; BD Biosciences Cat #553720), PE hamster IgG1 κ isotype control (1/16 dilution; BD Biosciences Cat #553972), BV421 rat anti-mouse CD5 (1/385 dilution; BD Biosciences Cat #562739), FITC rat anti-mouse CD45 (1/50 dilution; BD Biosciences Cat #553080), Alexa Fluor[®] 647 rat anti-mouse CD19 (1/135 dilution; BD Biosciences Cat #557684), LIVE/DEAD[™] fixable near-IR dead cell stain (1/165 dilution; ThermoFisher Scientific Cat #L34976), rat anti-mouse CD16/CD32 (1/100 dilution; Mouse BD Fc Block[™]; BD Biosciences Cat #553142), BV510 hamster anti-mouse CD3e (1/150 dilution; BD Biosciences Cat #563024), BV650 rat anti-mouse CD11-b (1/200 dilution; BD Biosciences Cat #653402), BB515 rat anti-mouse CD19 (1/200 dilution; BD Biosciences Cat #564509), BUV737 rat anti-mouse CD5 (1/150 dilution; BD Biosciences Cat #612809), APC rat anti-mouse CD93 (1/100 dilution; Biolegend Cat #136510), BUV395 rat anti-mouse CD45R/B220 (1/200 dilution; BD Biosciences Cat #563793), BV786 rat anti-mouse IgM (1/100 dilution; BD Biosciences Cat #564028), PerCP-Cy5.5 rat anti-mouse CD21 (1/200 dilution; Biolegend Cat #1234160), BV711 Rat anti-mouse CD23 (1/200 dilution; BD Biosciences Cat #563987), BV605 Rat anti-mouse IgD (1/100 dilution; BD Biosciences Cat #563003). Immunophenotyping was conducted using Beckman Coulter Gallios 3-laser-10-color (B5-R3-V2) cell analyzer and BD LSRFortessa Cell Analyzer (Cat #649225). Peripheral blood from E μ -MTCPI and E μ -TCL1 transgenic mice was collected monthly via cheek punch. Cells from the spleens of E μ -MTCPI and E μ -TCL1 having met predefined euthanasia criteria were processed and isolated using methods previously described. Mouse B cells were isolated from whole spleen suspensions using EasySep[™] mouse pan B cell isolation kit (STEMCELL Technologies; Cat #19844). All flow cytometry data were analyzed using KALUZA v2.0 software (Becton Dickinson).

Gating strategies followed published data and technical resource publications^{59–61} and were adapted to allow exclusion and interrogation of CD19⁺CD5⁺ CLL-like populations. Fluorescence-minus-one (FMO) controls were used for each marker and gate position. Cells were gated on viable single mononuclear cells.

Histopathology. To define the morphologic characteristics of tumor cells populating E μ -MTCPI mice, we performed histopathologic analysis on spleen, thymus, liver, mesenteric lymph node, and bone marrow. Organs were harvested from E μ -MTCPI mice meeting predefined euthanasia criteria and representative tissue samples were randomly selected from a pool of mice having evidence of a CLL-like disease. Tissues were fixed in 10% neutral buffered formalin (NBF). Bones were decalcified in formic acid (Surgipath). All tissues were embedded in paraffin and sectioned at 4 μ m onto glass slides. Stained sections were assessed by veterinary anatomic pathologists blinded to transgenic strain or treatment group (BH and JC). Staining with hematoxylin and eosin (H&E; Leica) F4/80, B220, and CD3 IHC were

described previously⁶². Photographs were taken using an Olympus SC30 camera with an Olympus BX53 microscope.

RNA-sequencing. Cell pellets were captured and washed in PBS on ice prior to resuspension in TRIzol reagent and stored at -80° . Total RNA was isolated from TRIzol suspensions using a chloroform/ethanol extraction method and quantified via Qubit RNA HS Assay kit (Invitrogen). The Clontech SMARTer v4 kit (Takara Bio USA, Inc.) was used for global preamplification. Illumina sequencing libraries were derived from the resultant cDNA using the Illumina Nextera XT DNA Library Prep Kit following manufacturer's instructions. RNA-sequencing libraries were prepared with the Illumina Tru-Seq stranded kit and sequenced on a HiSeq 4000 targeting 40×10^6 fragments per sample. Transcript-level abundances were estimated using Salmon⁶³ with the genome mouse release 23, imported using tximport⁶⁴, with normalization and differential expression computed with DESeq2⁶⁵. Data processing was performed according to the CLEAR workflow⁶⁶, which identifies reliably quantifiable transcripts in low-input RNA-seq for differentially expressed gene (DEG) transcripts using gene coverage profiles. MiXCR (v3.0.5)⁶⁷ was used with default parameters except the RNA-seq alignment was replaced with kaligner2 to identify preprocessed reads containing CDR3 regions from B-cell heavy, kappa, and lambda chains, generating a list of unique CDR3 sequences associated with their relative abundances and specific V(D)J gene usage. MiXCR then generates a list of unique CDR3 sequences associated with their relative abundances and specific V(D)J gene usage. To verify expression of the human *MTCPI* and *TCL1* transgene (*hMTCPI* & *hTCL1*) in mice, transcript level abundances were estimated using Salmon with a modified genome mouse reference that contained sequences from human *MTCPI* and human *TCL1* genes extracted from the grch38 human reference.

Therapeutic dosing in E μ -MTCPI mice. E μ -MTCPI littermate mice were randomized and enrolled to receive continuous ibrutinib (~30 mg/kg/day via drinking water) or vehicle administration beginning at 2 months of age orally via supplemented drinking water. Mice were followed for leukemia onset and overall survival until reaching predefined removal criteria.

Adoptive transfer studies were conducted using 1×10^6 viable E μ -MTCPI splenocytes injected via tail vein to immune competent C57BL/6NTac mice. Engrafted mice were monitored for leukemic expansion via weekly flow cytometry of peripheral blood collected by cheek punch. Upon reaching >20% CD45⁺/CD19⁺/CD5⁺ cells in peripheral blood mice were randomized and enrolled to receive either ibrutinib [25 mg/kg daily oral gavage (o.g.)] or vehicle (0.5% methylcellulose/1% Tween80 o.g.). Continued leukemia progression was monitored by weekly flow cytometry analysis of peripheral blood until reaching predefined removal criteria.

Statistics. Unless otherwise noted, analyses were performed by independent statisticians within the OSU Center for Biostatistics according to methods from previously described models. All analyses were performed using SAS/STAT software, version 9.4 (SAS Institute, Inc., Cary, NC). Evaluation of the difference in mean gene expression between cell types collected from the Blueprint DCC gene expression portal generated a two-tailed p value using an unpaired t test with Welch's correction.

For patient data, associations between *MTCPI* expression grouped by quartile and demographic, clinical, and molecular features were assessed using Fisher's exact and Kruskal-Wallis tests. *MTCPI* expression was correlated with PFS using a Cox stratified proportional hazards model, stratified on study cohort. Further modeling was performed controlling for other important demographic, clinical, or molecular variables. Multiple imputation estimated missing data and combined results for 20 datasets⁶⁸. All p values were two-sided and $p < 0.05$ were considered statistically

significant. No control for multiple comparisons were made. The correlation between *MTCP1* expression and PFS was visualized using Kaplan–Meier plots, grouping patients into quartiles according to *MTCP1* expression.

For mouse survival experiments, survival curve estimates for both overall survival and time to disease onset were calculated using the Kaplan–Meier method and differences in curves were initially assessed using the log-rank test. Next, hazard ratios (HR) and 95% CI were obtained from Cox proportional hazards models to evaluate differences between founder lines/E μ -TCL1 mice or treatment groups. Mixed effects models were used to assess changes in disease burden over time. Where applicable, data were log-transformed to reduce skewness.

Illustrations. Artistic renderings were created and exported under a paid subscription with Biorender.com. Biologic assembly of the proposed 3-dimensional structure of *MTCP1* and *TCL1* proteins, as determined by x-ray diffraction protein crystallography, was visualized and exported under a University supported subscription using the PYMOL Molecular Graphics System, Version 2.3.5. Unless otherwise noted, data were visualized using GraphPad Prism version 8.3.1 for Windows, GraphPad Software, San Diego, California USA.

Reporting summary. Further information on research design is available in the Nature Research Reporting Summary linked to this article.

Data availability

The RNA-sequencing data generated in this study have been deposited in the GEO database under accession code #GSE176094. The *MTCP1* expression and CLL patient outcomes data, from CALGB studies “10101” and “9712” used in this study, are not publicly available but can be accessed from the authors of these studies (CALGB “9712” - NCT00003248; CALGB “10101” - NCT00098670)^{27,28}. All other source data are provided as a Supplementary File. Source data are provided with this paper.

Received: 25 February 2021; Accepted: 21 September 2021;

Published online: 03 November 2021

References

- Hallek, M., Shanafelt, T. D. & Eichhorst, B. Chronic lymphocytic leukaemia. *Lancet* **391**, 1524–1537 (2018).
- Kikushige, Y. et al. Self-renewing hematopoietic stem cell is the primary target in pathogenesis of human chronic lymphocytic leukemia. *Cancer Cell* **20**, 246–259 (2011).
- Shanafelt, T. D. et al. B-cell count and survival: differentiating chronic lymphocytic leukemia from monoclonal B-cell lymphocytosis based on clinical outcome. *Blood* **113**, 4188–4196 (2009).
- Oakes, C. C. et al. DNA methylation dynamics during B cell maturation underlie a continuum of disease phenotypes in chronic lymphocytic leukemia. *Nat. Genet.* **48**, 253–264 (2016).
- Beekman, R. et al. The reference epigenome and regulatory chromatin landscape of chronic lymphocytic leukemia. *Nat. Med.* **24**, 868–880 (2018).
- Döhner, H. et al. Genomic aberrations and survival in chronic lymphocytic leukemia. *N. Engl. J. Med.* **343**, 1910–1916 (2000).
- Landau, D. A. et al. Mutations driving CLL and their evolution in progression and relapse. *Nature* **526**, 525–530 (2015).
- Pérez-Carretero, C. et al. Chronic lymphocytic leukemia patients with *IGH* translocations are characterized by a distinct genetic landscape with prognostic implications. *Int. J. Cancer* **147**, 2780–2792 (2020).
- Willis, T. G. & Dyer, M. J. The role of immunoglobulin translocations in the pathogenesis of B-cell malignancies. *Blood* **96**, 808–822 (2000).
- Adachi, M., Tefferi, A., Greipp, P. R., Kipps, T. J. & Tsujimoto, Y. Preferential linkage of *bcl-2* to immunoglobulin light chain gene in chronic lymphocytic leukemia. *J. Exp. Med.* **171**, 559–564 (1990).
- Kitada, S. et al. Expression of apoptosis-regulating proteins in chronic lymphocytic leukemia: correlations with *In vitro* and *In vivo* chemoresponses. *Blood* **91**, 3379–3389 (1998).
- Kimino, A. et al. *miR-15* and *miR-16* induce apoptosis by targeting *BCL2*. *Proc. Natl Acad. Sci. USA* **102**, 13944–13949 (2005).
- Klein, U. et al. The *DLEU2/miR-15a/16-1* cluster controls B cell proliferation and its deletion leads to chronic lymphocytic leukemia. *Cancer Cell* **17**, 28–40 (2010).
- Calin, G. A. et al. Frequent deletions and down-regulation of micro-RNA genes *miR15* and *miR16* at 13q14 in chronic lymphocytic leukemia. *Proc. Natl Acad. Sci. USA* **99**, 15524–15529 (2002).
- Souers, A. J. et al. ABT-199, a potent and selective *BCL-2* inhibitor, achieves antitumor activity while sparing platelets. *Nat. Med.* **19**, 202–208 (2013).
- Gritti, C. et al. Alternative origin of *p13^{MTCP1}*-encoding transcripts in mature T-cell proliferations with t(X;14) translocations. *Oncogene* **15**, 1329–1335 (1997).
- Yang, Y. S. et al. Solution structure of the recombinant human oncoprotein *p13^{MTCP1}*. *J. Biomol. NMR* **11**, 337–354 (1998).
- Hoh, F. et al. Crystal structure of *p14^{TCL1}*, an oncogene product involved in T-cell prolymphocytic leukemia, reveals a novel β -barrel topology. *Structure* **6**, 147–155 (1998).
- Fu, Z. Q. et al. Crystal structure of *MTCP-1*: implications for role of *TCL-1* and *MTCP-1* in T cell malignancies. *Proc. Natl Acad. Sci. USA* **95**, 3413–3418 (1998).
- Petock, J. M. et al. Crystal structures of *Tcl1* family oncoproteins and their conserved surface features. *ScientificWorldJournal* **2**, 1876–1884 (2002).
- Roumestand, C., Boyer, M., Guignard, L., Barthe, P. & Royer, C. A. Characterization of the folding and unfolding reactions of a small beta-barrel protein of novel topology, the *MTCP1* oncogene product *P13*. *J. Mol. Biol.* **312**, 247–259 (2001).
- Künstle, G. et al. Identification of Akt association and oligomerization domains of the Akt kinase coactivator *TCL1*. *Mol. Cell Biol.* **22**, 1513–1525 (2002).
- Stern, M. H. et al. *MTCP-1*: a novel gene on the human chromosome Xq28 translocated to the T cell receptor alpha/delta locus in mature T cell proliferations. *Oncogene* **8**, 2475–2483 (1993).
- Madani, A. et al. Expression of *p13^{MTCP1}* is restricted to mature T-cell proliferations with t(X;14) translocations. *Blood* **87**, 1923–1927 (1996).
- Gritti, C. et al. Transgenic mice for *MTCP1* develop T-cell prolymphocytic leukemia. *Blood* **92**, 368–373 (1998).
- Joiner, M., Le Toriellec, E., Despouy, G. & Stern, M. H. The *MTCP1* oncogene modifies T-cell homeostasis before leukemogenesis in transgenic mice. *Leukemia* **21**, 362–366 (2007).
- Woyach, J. A. et al. Chemoimmunotherapy with fludarabine and rituximab produces extended overall survival and progression-free survival in chronic lymphocytic leukemia: long-term follow-up of CALGB study 9712. *J. Clin. Oncol.* **29**, 1349–1355 (2011).
- Lin, T. S. et al. Consolidation therapy with subcutaneous alemtuzumab after fludarabine and rituximab induction therapy for previously untreated chronic lymphocytic leukemia: final analysis of CALGB 10101. *J. Clin. Oncol.* **28**, 4500–4506 (2010).
- Pekarsky, Y. et al. *Tcl1* functions as a transcriptional regulator and is directly involved in the pathogenesis of CLL. *Proc. Natl Acad. Sci. USA* **105**, 19643–19648 (2008).
- Cain-Hom, C. et al. Efficient mapping of transgene integration sites and local structural changes in Cre transgenic mice using targeted locus amplification. *Nucleic Acids Res.* **45**, e62 (2017).
- Bichi, R. et al. Human chronic lymphocytic leukemia modeled in mouse by targeted *TCL1* expression. *Proc. Natl Acad. Sci. USA* **99**, 6955–6960 (2002).
- Johnson, A. J. et al. Characterization of the *TCL-1* transgenic mouse as a preclinical drug development tool for human chronic lymphocytic leukemia. *Blood* **108**, 1334–1338 (2006).
- Kosmaczewska, A., Ciszak, L., Suwalska, K., Wolowicz, D. & Frydecka, I. *CTLA-4* overexpression in *CD19⁺/CD5⁺* cells correlates with the level of cell cycle regulators and disease progression in B-CLL patients. *Leukemia* **19**, 301–304 (2005).
- Do, P. et al. Leukemic B cell *CTLA-4* suppresses costimulation of T cells. *J. Immunol.* **202**, 2806–2816 (2019).
- Hao, X. et al. The histopathologic and molecular basis for the diagnosis of histiocytic sarcoma and histiocyte-associated lymphoma of mice. *Vet. Pathol.* **47**, 434–445 (2010).
- Blachly, J. S. et al. Immunoglobulin transcript sequence and somatic hypermutation computation from unselected RNA-seq reads in chronic lymphocytic leukemia. *Proc. Natl Acad. Sci. USA* **112**, 4322–4327 (2015).
- Ghia, P. et al. ERIC recommendations on *IGHV* gene mutational status analysis in chronic lymphocytic leukemia. *Leukemia* **21**, 1–3 (2007).
- Woyach, J. A. et al. Bruton’s tyrosine kinase (*BTk*) function is important to the development and expansion of chronic lymphocytic leukemia (CLL). *Blood* **123**, 1207–1213 (2014).
- Lee, J. T., Innes, D. J. & Williams, M. E. Sequential *bcl-2* and *c-myc* oncogene rearrangements associated with the clinical transformation of non-Hodgkin’s lymphoma. *J. Clin. Invest.* **84**, 1454–1459 (1989).
- Jares, P., Colomer, D. & Campo, E. Molecular pathogenesis of mantle cell lymphoma. *J. Clin. Invest.* **122**, 3416–3423 (2012).
- Pekarsky, Y. et al. *Tcl1* expression in chronic lymphocytic leukemia is regulated by *miR-29* and *miR-181*. *Cancer Res.* **66**, 11590–11593 (2006).
- Browning, R. L. et al. Expression of *TCL-1* as a potential prognostic factor for treatment outcome in B-cell chronic lymphocytic leukemia. *Leuk. Res.* **31**, 1737–1740 (2007).
- Herling, M. et al. *TCL1* shows a regulated expression pattern in chronic lymphocytic leukemia that correlates with molecular subtypes and proliferative state. *Leukemia* **20**, 280–285 (2006).
- Herling, M. et al. High *TCL1* levels are a marker of B-cell receptor pathway responsiveness and adverse outcome in chronic lymphocytic leukemia. *Blood* **114**, 4675–4686 (2009).

45. Balatti, V. et al. *TCL1* targeting *miR-3676* is codeleted with tumor protein p53 in chronic lymphocytic leukemia. *Proc. Natl Acad. Sci. USA* **112**, 2169–2174 (2015).
46. Holler, C. et al. PKC β is essential for the development of chronic lymphocytic leukemia in the *TCL1* transgenic mouse model: validation of PKC β as a therapeutic target in chronic lymphocytic leukemia. *Blood* **113**, 2791–2794 (2009).
47. Li, S. X. et al. Identification of a t(X;17)(q28;q21) generating a *KANSL1-MTCP1* gene fusion leading to dysregulated expression of *MTCP1* in acute myeloid leukemia. *Genes Chromosomes Cancer* **59**, 417–421 (2020).
48. Jonsson, D. I. et al. A *de novo* 1.13 Mb microdeletion in 12q13.13 associated with congenital distal arthrogyrosis, intellectual disability and mild dysmorphism. *Eur. J. Med. Genet.* **55**, 437–440 (2012).
49. Okamoto, N., Tamura, D., Nishimura, G., Shimojima, K. & Yamamoto, T. Submicroscopic deletion of 12q13 including *HOXC* gene cluster with skeletal anomalies and global developmental delay. *Am. J. Med. Genet. A* **155A**, 2997–3001 (2011).
50. Hancarova, M. et al. Chromosome 12q13.13 deletions involving the *HOXC* gene cluster: phenotype and candidate genes. *Eur. J. Med. Genet.* **56**, 171–173 (2013).
51. Dompe, N. et al. A whole-genome RNAi screen identifies an 8q22 gene cluster that inhibits death receptor-mediated apoptosis. *Proc. Natl Acad. Sci. USA* **108**, E943–51 (2011).
52. Crowther-Swanepoel, D. et al. Common variants at 2q37.3, 8q24.21, 15q21.3 and 16q24.1 influence chronic lymphocytic leukemia risk. *Nat. Genet.* **42**, 132–136 (2010).
53. Chapiro, E. et al. The most frequent t(14;19)(q32;q13)-positive B-cell malignancy corresponds to an aggressive subgroup of atypical chronic lymphocytic leukemia. *Leukemia* **22**, 2123–2127 (2008).
54. Huh, Y. O. et al. Chronic lymphocytic leukemia with t(14;19)(q32;q13) is characterized by atypical morphologic and immunophenotypic features and distinctive genetic features. *Am. J. Clin. Pathol.* **135**, 686–696 (2011).
55. Woyach, J. A. et al. Prolonged lymphocytosis during ibrutinib therapy is associated with distinct molecular characteristics and does not indicate a suboptimal response to therapy. *Blood* **123**, 1810–1817 (2014).
56. Madani, A. et al. The 8 kD product of the putative oncogene *MTCP-1* is a mitochondrial protein. *Oncogene* **10**, 2259–2262 (1995).
57. Burns, A. et al. Whole-genome sequencing of chronic lymphocytic leukaemia reveals distinct differences in the mutational landscape between IgHV^{unmut} and IgHV^{mut} subgroups. *Leukemia* **32**, 332–342 (2018).
58. Fernández, J. M. et al. The BLUEPRINT Data Analysis Portal. *Cell Syst.* **3**, 491–495.e495 (2016).
59. Becton, Dickinson & company. B-Cell Research. Flow cytometry tools for the study of B-cell biology. (2014).
60. Pieper, K., Grimbacher, B. & Eibel, H. B-cell biology and development. *J. Allergy Clin. Immunol.* **131**, 959–971 (2013).
61. Allman, D. & Pillai, S. Peripheral B cell subsets. *Curr. Opin. Immunol.* **20**, 149–157 (2008).
62. Lucas, F. et al. E μ -TCL1xMyc: a novel mouse model for concurrent CLL and B-cell lymphoma. *Clin. Cancer Res.* **25**, 6260–6273 (2019).
63. Patro, R., Duggal, G., Love, M. I., Irizarry, R. A. & Kingsford, C. Salmon provides fast and bias-aware quantification of transcript expression. *Nat. Methods* **14**, 417–419 (2017).
64. Soneson, C., Love, M. I. & Robinson, M. D. Differential analyses for RNA-seq: transcript-level estimates improve gene-level inferences. *F1000Res* **4**, 1521 (2015).
65. Love, M. I., Huber, W. & Anders, S. Moderated estimation of fold change and dispersion for RNA-seq data with DESeq2. *Genome Biol.* **15**, 550 (2014).
66. Walker, L. A. et al. CLEAR: coverage-based limiting-cell experiment analysis for RNA-seq. *J. Transl. Med.* **18**, 63 (2020).
67. Bolotin, D. A. et al. MiXCR: software for comprehensive adaptive immunity profiling. *Nat. Methods* **12**, 380–381 (2015).
68. van Buuren, S. Multiple imputation of discrete and continuous data by fully conditional specification. *Stat. Methods Med. Res.* **16**, 219–242 (2007).

Acknowledgements

We are grateful to the patients who provided blood for the above studies. Research support was provided in part by the National Cancer Institute of the National Institutes of Health (JSW: NIGMS T32 GM068412 and NCATS TL1 TR002735; JC: T32

CA009338). The content is solely the responsibility of the authors and does not necessarily represent the official views of the College of Medicine at The Ohio State University or the National Institutes of Health. This work was also supported in part by the Genetically Engineered Mouse Modeling Core (GEMMC) at the Ohio State University (funded by The OSU Comprehensive Cancer Center Support Grant P30 CA016058) for generation of the E μ -MTCP1 mouse model. The Ohio State University Comparative Pathology & Mouse Phenotyping Shared Resource (funded by a Cancer Center Support Grant P30 CA016058) supported pathology studies. Transcriptomic library generation and sequencing were supported by The Ohio State University Genomics Shared Resource (supported in part by a Cancer Center Support Grant P30 CA016058). Computational resources were provided by Ohio Supercomputer Center. This work was supported by the National Cancer Institute (R50 CA211524-03 and U54 CA217297 (PY), R35 CA197734 (JCB), R01 CA214046 (RL)). Support from Four Winds Foundation also supported this effort. This study makes use of data generated by the BLUEPRINT Consortium. A full list of the investigators who contributed to the generation of the data is available from www.blueprint-epigenome.eu. Funding for the project was provided by the European Union's Seventh Framework Program (FP7/2007–2013) under grant agreement no 282510 – BLUEPRINT.

Author contributions

J.S.W. and Z.A.H. designed and conducted experiments, generated data and figures, analyzed data, interpreted results, and wrote the paper. S.S., J.C., K.W., J.N.S., C.B.C., C.T.G., A.P., M.Y., and P.Y. conducted experiments and generated figures. J.C. and B.H. prepared and interpreted histopathology data. L.P.B. and B.R.W. performed animal experiments. Z.A.H., K.W., V.C., J.S.B., and R.L. contributed to the generation of the mouse model. J.M.L. and N.A.H. conducted and interpreted FISH analysis. K.M. and J.A.W. provided and interpreted CLL patient data. A.S.R., A.M.L., and H.G.O. conducted statistical analysis. J.S.B., J.C.B., and R.L. planned the project, acquired funding, supervised the study, interpreted results, and reviewed the paper. These senior authors (J.S.B., J.C.B., R.L.) contributed equally. All authors read and approved the final version of the paper.

Competing interests

J.S.B. has performed consulting for AbbVie, AstraZeneca, Innate, and KITE Pharma. J.C.B. performed consulting for AstraZeneca, Takada, Novartis, Pharmacyclis, Syndex, and Trillium. J.C.B. chairs the scientific board of Vincer Pharmaceuticals and has significant equity in this company. All other authors declare no competing interests.

Additional information

Supplementary information The online version contains supplementary material available at <https://doi.org/10.1038/s41467-021-26400-x>.

Correspondence and requests for materials should be addressed to Rosa Lalambella.

Peer review information *Nature Communications* thanks Alexander Egle and the other, anonymous, reviewer(s) for their contribution to the peer review of this work. Peer reviewer reports are available.

Reprints and permission information is available at <http://www.nature.com/reprints>

Publisher's note Springer Nature remains neutral with regard to jurisdictional claims in published maps and institutional affiliations.



Open Access This article is licensed under a Creative Commons Attribution 4.0 International License, which permits use, sharing, adaptation, distribution and reproduction in any medium or format, as long as you give appropriate credit to the original author(s) and the source, provide a link to the Creative Commons license, and indicate if changes were made. The images or other third party material in this article are included in the article's Creative Commons license, unless indicated otherwise in a credit line to the material. If material is not included in the article's Creative Commons license and your intended use is not permitted by statutory regulation or exceeds the permitted use, you will need to obtain permission directly from the copyright holder. To view a copy of this license, visit <http://creativecommons.org/licenses/by/4.0/>.

© The Author(s) 2021